NsG 382

[redacted]

48p

VELOCITY DISTRIBUTIONS OF THE INTERPLANETARY PLASMA DETECTED BY EXPLORER 10*

CR55557

by

F. Scherb [1963] 48p xerox

Physics Department and Laboratory for Nuclear Science
Massachusetts Institute of Technology
Cambridge, Massachusetts

1486984

(NASA Grant NsG -386)
(Sponsored by NASA)
(NASA CR-55557)

FACILITY FORM 602

N65 16492 (ACCESSION NUMBER) — (THRU)
48 (PAGES) — 1 (CODE)
CR 55557 (NASA CR OR TMX OR AD NUMBER) — 25 (CATEGORY)

* This work was supported in part by the National Aeronautics and Space Administration and the United States Atomic Energy Commission.

GPO PRICE $ _____

OTS PRICE(S) $ _____

Hard copy (HC) 2.00

Microfiche (MF) .50

[redacted]

I. Introduction

The Explorer 10 satellite (launched 1517 UT, 25 March, 1961) carried out measurements on magnetic fields and plasma for about 50 hours along a trajectory that extended to an apogee of 47 earth radii. Extensive reports on the flight and the experimental results have already been presented. In particular a detailed description of the magnetic field measurements has been published by Heppner, et al (Heppner, Ness, Skillman and Scearce, 1963) and a recent paper by Bonetti, et al (Bonetti, Bridge, Lazarus, Rossi and Scherb) describes the plasma measurements. We shall refer to the latter paper as BBLRS.

The purpose of this paper is to present the results of an analysis of the plasma data with regard to the velocity distribution and angular distribution of the plasma ions.

We shall first review briefly the plasma probe instrumentation and measurement procedure, which are described in detail in BBLRS.

Fig. 1 shows a schematic diagram of the plasma cup and a block diagram of the electronics. Positively charged ions incident on the cup at an angle δ to the cup normal $\vec{n}$ were detected by the A.C. measurement chain if they were modulated by grid G_2 which acted as an electrical gate. The modulator circuit applied a voltage to G_2 in the form of a square wave which oscillated between zero volts and + V_m volts at a frequency of 1400 cps. Thus positive

ions with an energy-to-charge ratio E/q in the range given by

$$E/q \leq V_m \cos^{-2} \delta \qquad (1)$$

produced at the collector plate CP a pulsating current whose A.C. component was fed into the A.C. measurement chain through the coupling capacitor C. The D.C. component of the collector plate current was fed into a simple D.C. amplifier which was intended to provide auxiliary information about the ion currents, photoelectric currents, and any other direct currents at the collector plate.

The plasma cup was located on Explorer 10 so that the cup normal $\vec{n}$ was perpendicular to the spin axis, as shown in Fig. 2. Thus an azimuthal scan was provided by the rotation of the satellite, whose spin period was 548 milliseconds.

Fig. 3a shows the Explorer 10 telemetry sequence and Fig. 3b shows the plasma measurement cycle. It can be seen that each successive plasma measurement, lasting for 5 seconds (about 9 rotations of the satellite), was carried out in one of 8 different modes. The marker mode and D.C. mode provided no information about the plasma and will not be described here.

Fig. 4 shows the telemetry signals obtained in the sequence of measurements carried out between 0831 and 0843 UT, 26 March, when Explorer 10

was at a geocentric distance of about 25 earth radii. The times when the normal $\vec{n}$ to the plasma cup rotated into the plane containing the spin axis and the satellite-sun direction are indicated by vertical lines some of which are labelled "SUN TIME". (This sequence was selected for analysis because the telemetered signals were unusually free of radio noise which often obscured the plasma probe signal shapes to such an extent that a detailed analysis was not feasible.)

Since the satellite spin provided as many as 8 or 9 plasma signal pulses during a 5-second measurement period, individual pulses have been superposed to reveal average shapes more clearly, and the results are shown in Fig. 5 (the pulses were superposed by making the sun times coincide). The pulse shapes are quite clear although telemetry noise has obscured to some extent the leading slopes.

Fig. 6 shows some geometrical relationships involved in the analysis of the motions of the plasma ions. The coordinate system has been chosen so that the z-axis is along the spin axis of the satellite and the x-z plane contains the direction to the sun. The plasma cup normal $\vec{n}$ rotates in the x-y plane and γ is the angle it makes with the x-axis. The sun-time is given by the instant when $\vec{n}$ coincides with the x-axis (i.e., $\gamma = 0$). The vector $\vec{v}$ represents the velocity of ions incident at an angle α to the x-y plane. The angle δ between $\vec{v}$ and $\vec{n}$ is given by

$$\cos \delta = \cos \alpha \cos \beta \qquad (2)$$

where β is the angle between $\vec{n}$ and the projection of $\vec{v}$ in the x-y plane.

Fig. 7a shows the A.C. signal from the plasma cup as a function of δ for ions whose energy-to-charge ratio E/q is smaller than the modulating voltage amplitude V_m. When E/q is greater than V_m, the ion current is not modulated until δ exceeds a critical value δ_c given by

$$\delta_c = \cos^{-1}\left(\frac{V_m}{E/q}\right)^{1/2} \quad . \tag{3}$$

This is illustrated in Fig. 7b which shows the cup response for $E/q = 1.2\ V_m$.

It is more convenient for comparison with the telemetry signals to plot the cup response as a function of the angle β. Thus Fig. 8 shows a set of such curves (normalized to unity at $\beta = 0$) which have been obtained from Fig. 7a and Eq. 2. These curves show how the shape of the output signal from the cup depends on the angle of incidence α for a parallel beam of particles with $(E/q)\cos^2\alpha \leq V_m$. Since most of the particles detected by the Explorer 10 plasma probe had $(E/q)\cos^2\alpha$ smaller than 800 volts and certainly well below 2300 volts, it would be useful to compare the curves in Fig. 8 with the 2300-volt telemetry signal shown in Fig. 5d.

But we must first correct for the distortion of the signals due to the plasma probe electronics. There were two significant sources of distortion: (1) The compression amplifier in the A.C. measurement chain (see Fig. 1) had

a nonlinear gain characteristic as shown in Fig. 9. Thus the distortion was a function of the height of the signal and was more serious for large signals such as those obtained at the 800-volt or 2300-volt modulation levels than for smaller signals like those obtained at the 250-volt modulation level. (2) The low-pass filter at the end of the A.C. measurement chain acted as an integrator with a time constant of 15 milliseconds. This caused a delay of the telemetry signal relative to the cup signal by about 15 milliseconds (or 10° of vehicle rotation) with negligible distortion of the pulse shapes (see Fig. 16).

An example of the effect of the A.C. measurement chain on a signal is illustrated in Fig. 10 where the input signal represents the cup response function for $\alpha = 0^{\circ}$ with the time scale adjusted to correspond to the Explorer 10 spin rate. The peak height of the output signal is the same as the peak height of the signal shown in Fig. 5d.

II. Velocity Distribution of the Plasma Ions

We assume that in a frame of reference that moves with the bulk velocity of the plasma, the ions have an isotropic Maxwellian velocity distribution characterized by a temperature T. We choose this simple model because it is convenient and not because there is any strong reason to believe that it is an adequate description of the actual ion velocity distribution. Indeed, one might expect that there would be some degree of anisotropy with respect to the direction of the magnetic field associated with the plasma, since

ordinary randomizing collisions between the particles are virtually absent. However, it is useful to try first a simple, isotropic distribution, since the plasma probe data probably do not justify using a more complicated one.

Thus in the x-y-z frame of reference shown in Fig. 6, the number of particles per cm^3 having speeds between v and v + dv and moving in directions within the solid angle $d\Omega$ about the direction of the velocity vector $\vec{v}$ is

$$f(v)dv\, d\Omega = n(m/2\pi kT)^{3/2} \exp\left[-m(\vec{v}-\vec{v}_o)^2/2kT\right] v^2\, dv\, d\Omega \qquad (4)$$

where $\vec{v}_o$ is the bulk velocity, n is the total ion density, m is the ion mass[1], and k is the Boltzmann constant.

The number of particles per second which cross an area of one cm^2 that is oriented perpendicular to $\vec{v}$ and which have speeds between v and v + dv is given by

$$\phi(v)dv\, d\Omega = v\, f(v)dv\, d\Omega \quad . \qquad (5)$$

We shall call $\phi(v)dv\, d\Omega$ the differential flux density.

The net number of particles per second which cross an area of one cm^2 that is oriented perpendicular to $\vec{v}_o$ is given by

$$\Phi(v_o) = n\, v_o \quad . \qquad (6)$$

---

1 We will assume that the positive ion component of the plasma consists only of protons.

We shall call $\Phi(v_o)$ the total flux density.

In order to compute the cup signal, it is necessary to specify the ion temperature T and the bulk velocity v_o. We will use the same symbols α and β for the angles specifying the direction of $\vec{v}_o$ relative to $\vec{n}$ (see Fig. 6) as were used to specify the direction of $\vec{v}$ relative to $\vec{n}$. Since $\vec{n}$ rotates in the x-y plane, only the angle α needs to be specified. Thus the cup signal is computed as a function of the angle β for given values of T, v_o and α (it will usually be more convenient to use the kinetic energy of bulk motion $E_o = mv_o^2/2$ instead of v_o in presenting the results).

We omit here the details of the computations of the cup signals, which involve rather complicated integrations over the differential flux density given by Eq. 5 and the cup response function shown in Fig. 7. Fig. 11 shows the results of such a calculation for the case of $\alpha = 0^o$, $T = 6 \times 10^5\ ^oK$ and $E_o = 450$ ev. The curves have been normalized so that the signal for the 2300-volt modulation level is unity at $\beta = 0^o$. Thus the heights of the normalized signals at $\beta = 0^o$ for the 250-volt and 800-volt modulation levels correspond respectively to the relative flux densities denoted in BBLRS by $\bar{\Phi}(250)/\bar{\Phi}(2300)$ and $\bar{\Phi}(800)/\bar{\Phi}(2300)$. The results presented in Table 5 of BBLRS have been used as a guide for choosing values of T and E_o in the calculations. For example, during intervals No. 2, 4, 6, 10b and 10c (see BBLRS) the average flux densities gave the following ratios: $\bar{\bar{\Phi}}(250)/\bar{\bar{\Phi}}(2300) = 0.12$, $\bar{\bar{\Phi}}(800)/\bar{\bar{\Phi}}(2300) = 0.88$. Fig. 12 shows

ratios obtained from the computed curves at $\beta = 0^{\circ}$ for various values of T and E_o and for $\alpha = 0^{\circ}$. We consider the computed ratios that fall within the bands indicated by the dashed lines to be in reasonable agreement with the experimental ratios. Similar graphs for the computed ratios have been obtained for $\alpha = 20^{\circ}$, $\alpha = 40^{\circ}$ and $\alpha = 60^{\circ}$ but we omit them here.

The temperatures and bulk energies which give acceptable ratios of the pulse heights at $\beta = 0^{\circ}$ depend on the angle α . Thus the problem of determining the temperature cannot be separated from the problem of determining the average arrival direction of the plasma and the magnitude of the bulk velocity.

We showed previously (see Fig. 8) that the shape of the cup signal depends on α when the incident ions form a parallel beam. For example, if the ions were all incident at $\alpha = 60^{\circ}$ and if they were fully modulated at all values of β , then the cup signal would be significantly narrower than the signal for $\alpha = 0^{\circ}$. However, when there is a significant spread in the arrival directions of the ions, due to random motions transverse to the bulk velocity, the shapes of the cup signals may not be very sensitive to the value of α , as shown in Figs. 13 and 14 for the 800-volt and 2300-volt modulation levels. These figures summarize the results of pulse-shape calculations for various values of T and E_o at $\alpha = 0^{\circ}$, 20°, 40°, and 60°. Since the individual curves in each group lie quite close to each other, they have been replaced by shaded strips which indicate the variations in pulse shapes for each value of α . The dashed curves represent

the cup response function for $\alpha = 0^{o}$. It is evident that there is virtually no significant variation in the pulse shapes associated with different values of α . Thus we cannot use the measurements obtained at the 800-volt and 2300-volt modulation levels for the purpose of putting limits on the range of α .

The pulse shapes for the 250-volt measurement level are somewhat more sensitive to the value of α , as Fig. 15 shows. The main reason for the variety of signal shapes obtainable at this modulation level is the fact that the ion energy spectrum rises rapidly with increasing energy in the range around E = 250 ev. As the satellite rotates, the plasma cup modulation grid modulates those incident ions whose energies are smaller than a value E' given by

$$E' \leq qV_m \cos^{-2} \alpha \cos^{-2} \beta \quad . \tag{7}$$

Since E' goes through a minimum at $\beta = 0^{o}$, there is a corresponding tendency for the cup signal to go through a minimum at $\beta = 0^{o}$. Of course, the signal must also go to zero at those values of β where the cup response is zero. Thus the signals can acquire "horns" as shown in Fig. 15a and 15b for $\alpha = 0^{o}$ and $\alpha = 20^{o}$, but Fig. 15c and 15d show that for $\alpha \geq 40^{o}$ the signals do not have "horns" for the range of temperatures and bulk velocities being considered here.

By comparing the signals obtained at the 250-volt level with curves like

those shown in Fig. 15, we can set an upper limit to α . The validity of such a comparison depends on the amount of distortion caused by the plasma probe electronics, particularly the low-pass filter (the compression amplifier did not significantly distort the signals obtained at the 250-volt modulation level because the amplitudes of these signals were in the range where the amplifier was approximately linear). To test this, we simulated various types of cup signals using a function generator and passed them through a circuit which produced the same effect as the low-pass filter. Fig. 16 shows oscilloscope pictures of the results for three distinct pulse shapes. It is clear that the low-pass filter did not seriously change the signal shapes, except for introducing a delay. Thus the observed signals at the 250-volt level can be compared directly with the computed curves. However, it is necessary to adjust the shape of the computed 800-volt and 2300-volt curves before they can be compared with the corresponding signals since there was significant compression of these larger signals by the amplifier.

Fig. 17 shows that the observed 250-volt pulses are not consistent with a value of α as large as 40°. Presumably, any value of α smaller than about 30° would be an acceptable choice, and in the following discussion, we will assume for convenience that $\alpha = 0^{\circ}$. Thus the following results will correspond to this choice and should be regarded as nominal values for the temperature and bulk velocity.

Fig. 18 provides visual comparisons between the observed pulse shapes and computed pulse shapes for the 250-volt modulation level. It can be seen that some of the computed curves differ significantly in shape from the observed signals, and thus can be regarded as incompatible with the observations. If we use the rather qualitative selection criterion of requiring a reasonable visual agreement between the computed curves and the observed signals, we conclude that the range of nominal temperatures and the range of nominal energies which satisfy this criterion are the following:

$$\begin{aligned} 5 \times 10^5\ ^\circ K \leq T &\leq 8 \times 10^5\ ^\circ K \\ 400 \quad ev \leq E_o &\leq 450\ ev \quad . \end{aligned} \tag{8}$$

The limits on E_o correspond to 277 km sec^{-1} and 294 km sec^{-1} respectively for the proton bulk velocity.

It was noted earlier that the curves obtained for the 800-volt and 2300-volt modulation levels do not exhibit enough variation in shape to be used for an independent determination of T and E_o . However, they are useful for testing the validity of the results obtained above. Fig. 19 compares the observed pulses for these levels with computed curves corresponding to $T = 5 \times 10^5\ ^\circ K$ and $T = 8 \times 10^5\ ^\circ K$, respectively, with the energy E_o in the range given by Eq. 8 (there is essentially no variation in shape for different values of E_o in this range). It can be seen that $T = 8 \times 10^5\ ^\circ K$ gives a slightly better fit to the measurements than $T = 5 \times 10^5\ ^\circ K$, but this result

may not be very significant, in view of the instrumental effects discussed earlier (it should be noted that the computed curves in Fig. 19 have been compressed according to the amplifier response curve given in Fig. 9). The main conclusion we infer from these curves is that the model used in the calculations gives reasonably good agreement with the data discussed up to this point.

However, we find a discrepancy between the calculated signals and the observations for the 80-volt modulation level. The calculated signals, although similar in shape to the observed signals shown in Fig. 5a, are so small in magnitude relative to the signals at the higher modulation levels that they would not appear above the noise level of the amplifier. Thus the appearance of a definite signal at the 80-volt level, as shown in Fig. 5a, indicates that there were more low-energy ions in the plasma than would be expected if the ion velocity distribution were strictly Maxwellian.

As discussed in BBLRS, the plasma observed during the flight of Explorer 10 exhibited variations in its average properties. For example, there were intervals during which the "temperature" was lower than during other intervals (see BBLRS for a detailed discussion of these intervals). The results we have presented so far correspond to one of the so-called "high-temperature" intervals. Fig. 20 shows composite signals obtained from a measurement sequence in one of the "low-temperature" intervals (no signals were observed at the 80-volt modulation level or at the lower levels immediately preceeding these measurements). An analysis similar to the one described above was carried out

for these measurements and the results are presented in Figs. 21, 22, and 23. The relative pulse heights for the 250-volt and 800-volt modulation levels are plotted as functions of T and E_o in Fig. 21, and in the same fashion as discussed previously, we consider the pulse heights that fall within the bands indicated by the dashed lines to be in reasonable agreement with the observed signals (see Table 5 of BBLRS). Thus the experimental ratios have been used as guides for choosing the values of T and E_o in the computations of the pulse shapes shown in Figs. 22 and 23.

An inspection of Figs. 21 and 22 yields the following approximate limits for T, E_o, and v_o:

$$\begin{aligned} 3 \times 10^5\ ^oK \leq T &\leq 5 \times 10^5\ ^oK \\ 390\ \text{ev} \leq E_o &\leq 420\ \text{ev} \\ 273\ \text{km sec}^{-1} \leq v_o &\leq 284\ \text{km sec}^{-1} \end{aligned} \qquad (9)$$

Thus the plasma bulk velocity is about the same as it was in the previous case, but the temperature limits are somewhat lower than the previous values.

Fig. 23a shows that the signals obtained at the 800-volt modulation level are not quite consistent in shape with the theoretical signals that correspond to the values of T and E_o given above. This discrepancy could be removed by increasing E_o somewhat, but then the calculated signals for the 250-volt level would become much smaller than the observed signals. If we speculate that the

rather small signals observed at the 250-volt level may have been due to a non-Maxwellian component of the plasma and consequently should not be considered in the calculations, then we could try to determine the approximate temperature and bulk velocity of the ions using only the signals obtained at the 800-volt and 2300-volt modulation levels. We have not done this yet, but the results probably would not differ significantly from those given in Eq. 9 .

For a period of about one hour following a magnetic storm commencement at $15^h\ 03^m$ UT, 27 March (see BBLRS and Heppner, Ness, Skillman, and Scearce, 1963), the ion energy distribution shifted to higher energies and the total flux of ions increased (afterward, the plasma returned to its pre-storm condition). Fig. 24 shows composite signals obtained from a plasma measurement sequence carried out during this period, and the results of the pulse-shape calculations are shown in Figs. 25, 26 and 27.

It can be seen that the results of these calculations are not quite consistent with the observed signals. Those computed curves in Fig. 26 which fit reasonably well the observed pulses correspond to the following values of T, E_o and v_o :

$$\begin{aligned} 4 \times 10^5\ ^oK \leq T &\leq 5 \times 10^5\ ^oK \\ 950\ \text{ev} \leq E_o &\leq 1000\ \text{ev} \\ 427\ \text{km sec}^{-1} \leq v_o &\leq 438\ \text{km sec}^{-1} \end{aligned} \qquad (10)$$

However, Fig. 25 shows that these values of T and E_o give normalized pulse heights at $\beta = 0^o$ which lie below the acceptable range of values. Thus we conclude that the simple theoretical model used in these calculations is not quite adequate to account for both the shape and height of the signals obtained at the 800-volt and 2300-volt levels.

There is also a discrepancy between the computed signals and the observed signals for the 250-volt modulation level. The computed signals corresponding to the values of T and E_o given in Eq. 10 are negligibly small, whereas Fig. 24a shows that a definite signal was obtained, indicating again the existence of a non-Maxwellian, low-energy component in the plasma.

III. Discussion

The temperatures derived from the Explorer 10 plasma probe data refer only to the positive-ion component of the plasma. There was no information obtained on the plasma electrons, which did not necessarily have the same temperature as the ions. If we assume that the electron temperature T_e was about the same as the ion temperature T_i , then an interesting problem arises in connection with the tendency for the satellite to acquire a negative charge due to the higher random velocities of the electrons. The satellite could conceivably reach a negative potential of the order of a few times kT_i/e , where k is the Boltzmann constant and e is the elementary unit of charge. In the absence of other effects, such as solar ultra-violet photoeffect, which tend to produce a positive charge on the vehicle, the satellite potential with respect to the neutral plasma might be the order of - 100 volts. This would have

a significant effect on low-energy ions incident on the plasma probe and thus create uncertainties in the interpretation of the plasma data. However, the general character of the signals from the Explorer 10 plasma probe, particularly the absence of signals at the lowest modulation levels and the high degree of collimation in arrival directions, suggests that there was not a significant negative charge on the satellite, presumably because the solar photoeffect cancelled the effect of the plasma electrons. In fact, the satellite may have had a small positive potential with respect to the plasma due to the photoeffect.

It seems that attempts to make direct measurements of vehicle charge in this environment would be useful, since it is a very difficult problem to analyze theoretically, and the validity of simplified theoretical analyses may be limited to rather special cases.

REFERENCES

Bonetti, A., H. S. Bridge, A. J. Lazarus, B. Rossi and F. Scherb, Explorer 10 Plasma Measurements, paper to be published in the Journal of Geophysical Research.

Heppner, J. P., N. F. Ness, C. S. Scearce and T. L. Skillman, Explorer 10 Magnetic Field Measurements, J. Geophys. Research 68 (1963), pp. 1-46.

FIGURE CAPTIONS

Fig. 1. Schematic diagram of the plasma probe and block diagram of the electronic system.

Fig. 2. The Explorer 10 satellite.

Fig. 3. (a) The Explorer 10 telemetry sequence.
(b) The plasma measurement cycle.

Fig. 4. Plasma probe telemetry records for the sequence of six measurements carried out between 08^h31^m and 08^h43^m UT, 26 March. The vertical lines represent times when the normal to the cup was closest to the direction of the sun-satellite line; hence the designation "Sun Time". The distance between two consecutive vertical lines represents a single rotation period of 548 milliseconds.

Fig. 5. Composite signals obtained by superposing some of the individual pulses shown in Fig. 4. The pulses were superposed by making the sun times coincide. The sun time is indicated by the short vertical line above each composite pulse.

Fig. 6. The coordinate system used to represent the various vectors and angles involved in describing the motions of the plasma ions.

Fig. 7. (a) The normalized plasma cup response function for a parallel beam of ions whose energy-to-charge ratio E/q is smaller than V_m (i.e., the ion beam is fully modulated).

(b) The cup response function for $E/q = 1.2\ V_m$ (partial modulation).

Fig. 8. Response curves of the plasma probe plotted as functions of β for different values of α. The curves have been normalized to unity at $\beta = 0^o$.

Fig. 9. Nonlinear gain characteristic of the compression amplifier.

Fig. 10. An example of signal distortion due to the non-linearity of the compression amplifier and the time delay in the low-pass filter.

Fig. 11. Computed pulse shapes for the 250-volt, 800-volt and 2300-volt modulation levels. The curves are normalized so that the signal for the 2300-volt level is unity at $\beta = 0^{o}$.

Fig. 12. The solid curves in the upper part of the figure give the computed pulse heights at $\beta = 0^{o}$ for the 800-volt modulation level. The lower set of curves give the pulse heights at $\beta = 0^{o}$ for the 250-volt level. The ordinate gives pulse height as a percentage of the pulse height for the 2300-volt level at $\beta = 0^{o}$. The abscissa is the kinetic energy of bulk motion (for protons) and the numbers by the curves give the temperature in units of $10^{5}{}^{o}$K. The dashed lines define the ranges in which the computed pulse heights are considered to be reasonably consistent with the Explorer 10 measurements.

Fig. 13. Computed pulse shapes for the 800-volt modulation level. The different values of T (in units of $10^{5}{}^{o}$K) and E_{o} (in ev) selected for each value of α are given at the upper left of each figure. Since the individual curves lie quite close together, they have been replaced by shaded strips. For comparison, the dashed curves show the cup response function for $\alpha = 0^{o}$ (see Fig. 7a).

Fig. 14. Same as Fig. 13 for the 2300-volt modulation level.

Fig. 15. Same as Fig. 13 for the 250-volt modulation level, except that for $\alpha = 0^{o}$, the individual curves are shown rather than being replaced by a shaded strip.

Fig. 16. Oscilloscope photographs showing the effect of the low-pass filter on various signal shapes:
(a) The upper curve is the input signal to the low-pass filter and the curve below it is the output signal. A 60-cps sign wave is also shown for time-scale calibration.

(b) The upper curve is the input signal to the low-pass filter and the lower curve is the output signal.

(c) The input and output signals are displayed so as to show clearly the delay introduced by the low-pass filter.

Fig. 17. Comparison between the signals obtained at the 250-volt modulation level (Fig. 5b) and pulse shapes computed for $\alpha = 40^{o}$ (see Fig. 15c). The individual computed curves have been replaced by a shaded strip which indicates the range over which the pulse shapes vary.

Fig. 18. Comparison between the signals obtained at the 250-volt modulation level (Fig. 5b) and pulse shapes computed for $\alpha = 0^{o}$. The numbers by the curves correspond to the following values of E_{o}:

1 - E_{o} = 350 ev
2 - E_{o} = 400 ev
3 - E_{o} = 450 ev
4 - E_{o} = 500 ev

Fig. 19. Comparison between the signals obtained at the 800-volt and 2300-volt modulation levels (Fig. 5c and 5d) and computed pulse shapes.

Fig. 20. Composite signals obtained from the plasma measurements carried out between 03^h03^m and 03^h08^m, 27 March. The sun time is indicated by the short vertical line above each composite pulse.

Fig. 21. These results apply to the pulses shown in Fig. 20. They correspond to the results given in Fig. 12 for the pulses shown in Fig. 5. See the Fig. 12 caption for an explanation.

Fig. 22. Comparison between the signals obtained at the 250-volt modulation level (Fig. 20a) and pulse shapes computed for $\alpha = 0^o$. The numbers by the curves correspond to the following values of E_o:

1 - E_o = 350 ev
2 - E_o = 400 ev
3 - E_o = 450 ev

Fig. 23. Comparison between the signals obtained at the 800-volt and 2300-volt modulation levels (Fig. 20b and 20c) and computed pulse shapes.

Fig. 24. Composite signals obtained from the measurements carried out between 16^h31^m and 16^h37^m, 27 March. (only one pulse was obtained at the 2300-volt level). The sun time is indicated by the short vertical line above each composite pulse.

Fig. 25. These results apply to the pulses shown in Fig. 24. See the Fig. 5 and Fig. 21 captions for an explanation.

Fig. 26. Comparison between the signals obtained at the 800-volt modulation level (Fig. 24b) and pulse shapes computed for $\alpha = 0^o$. The numbers by the curves correspond to the following values of E_o:

1 - E_o = 850 ev
2 - E_o = 900 ev
3 - E_o = 950 ev
4 - E_o = 1000 ev

Fig. 27. Comparison between the signal obtained at the 2300-volt modulation level (Fig. 24c) and computed pulse shapes.

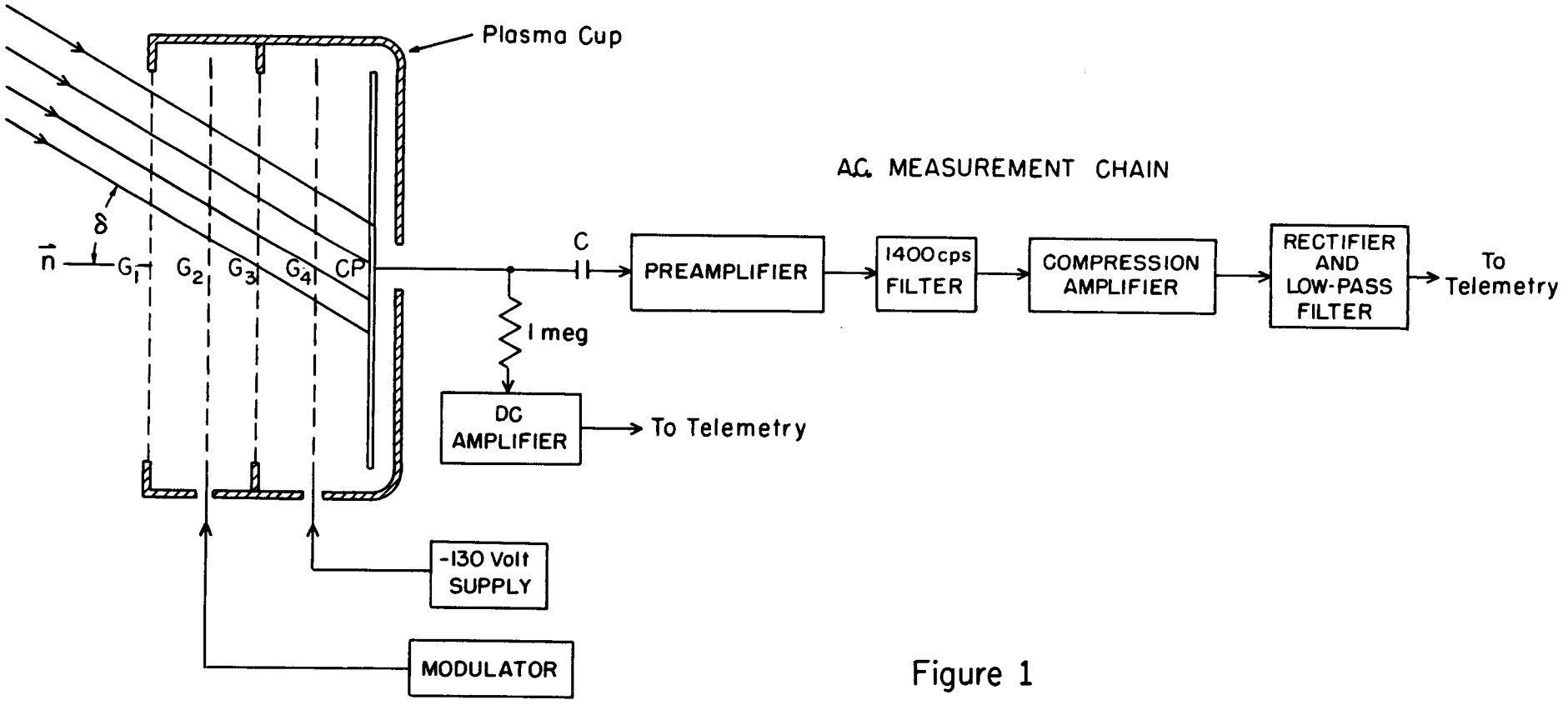
Plasma Cup
δ
n
G1
G2
G3
G4
CP
C
1 meg
DC AMPLIFIER
To Telemetry
-130 Volt SUPPLY
MODULATOR
A.C. MEASUREMENT CHAIN
PREAMPLIFIER
1400cps FILTER
COMPRESSION AMPLIFIER
RECTIFIER AND LOW-PASS FILTER
To Telemetry

Figure 1

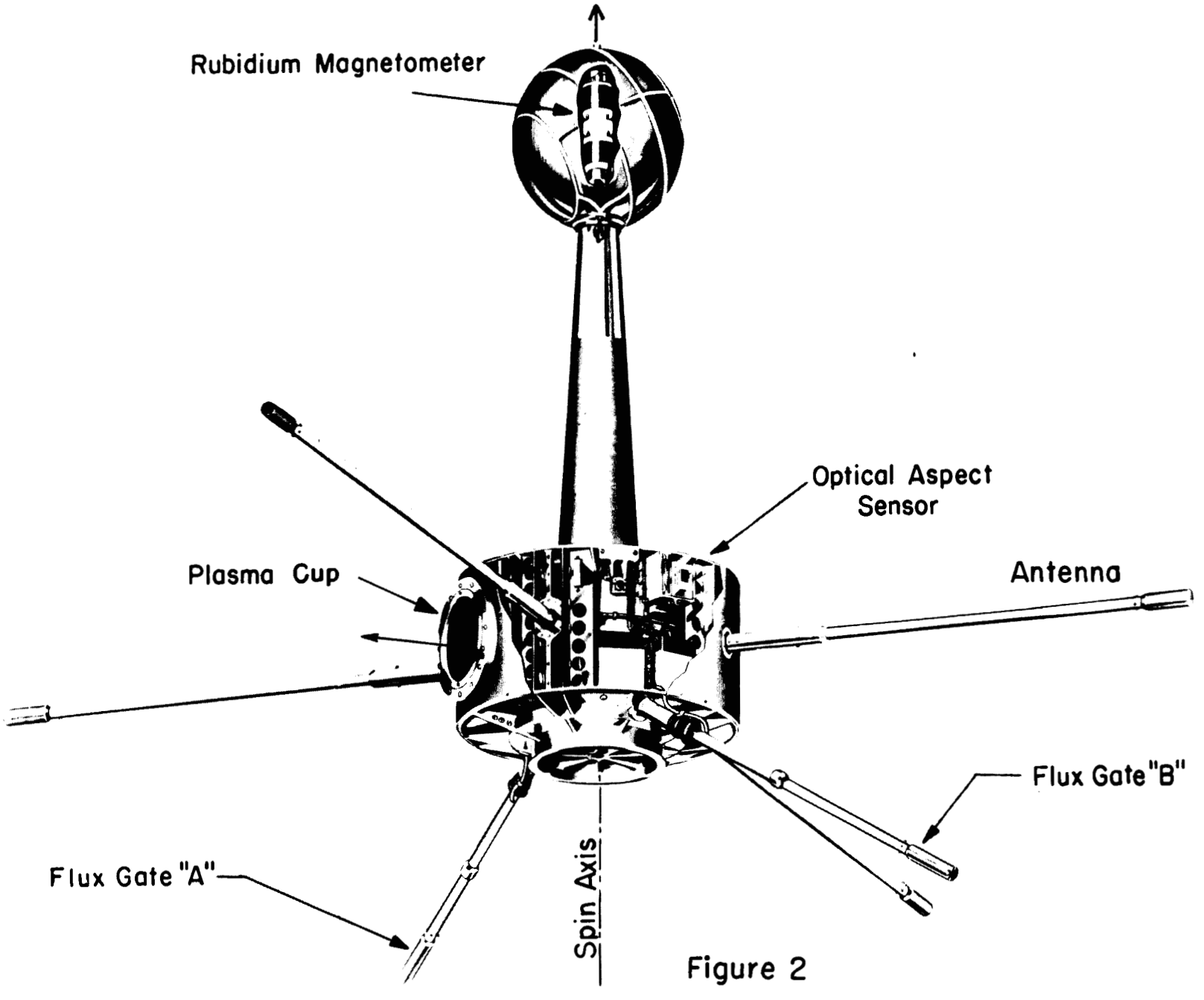
Rubidium Magnetometer
Optical Aspect Sensor
Plasma Cup
Antenna
Flux Gate "B"
Flux Gate "A"
Spin Axis

Figure 2

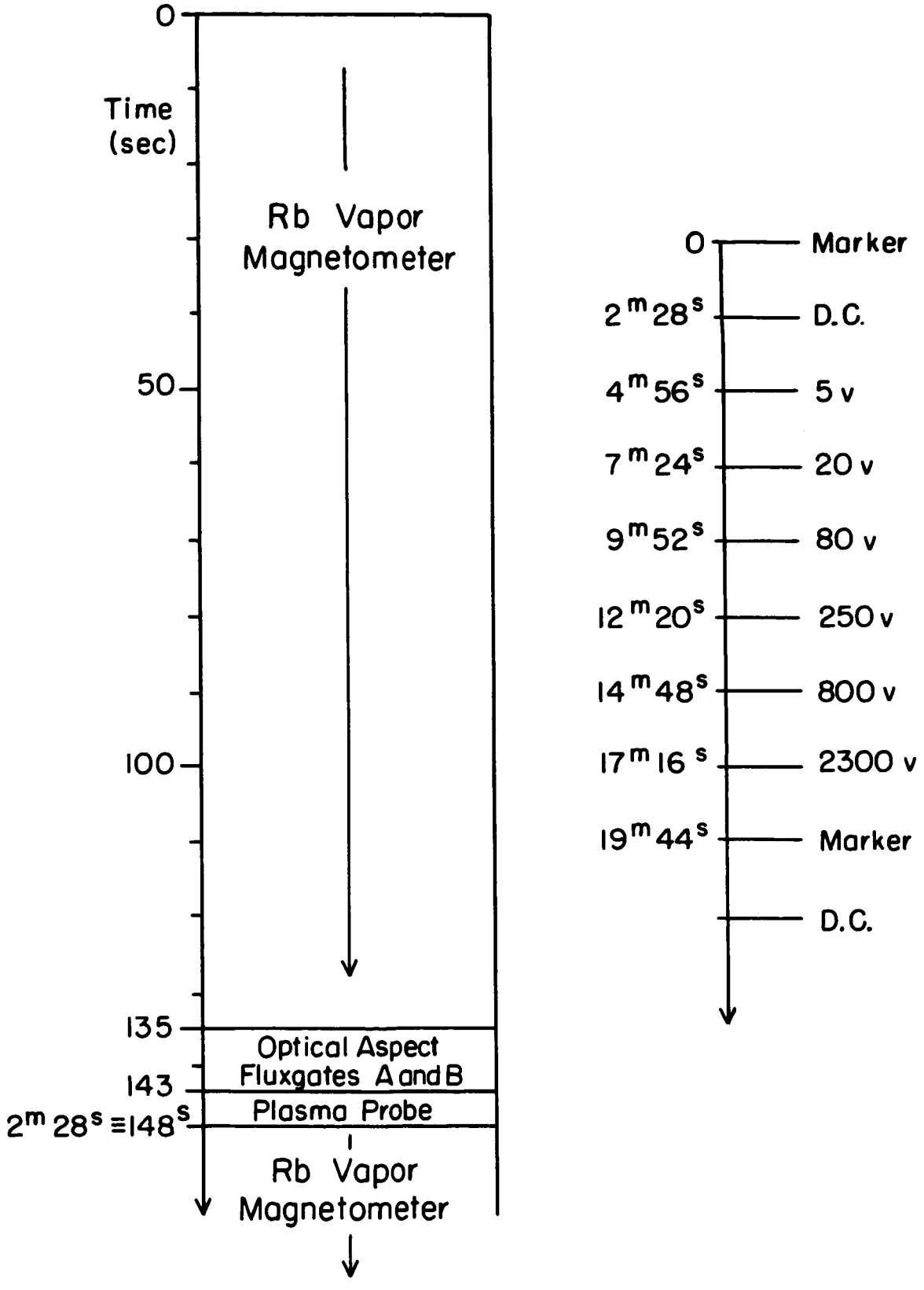
0
Time
(sec)
Rb Vapor
Magnetometer
50
100
135
Optical Aspect
Fluxgates A and B
143
Plasma Probe
2m 28s ≡148s
Rb Vapor
Magnetometer
(a)
0
Marker
2m 28s
D.C.
4m 56s
5 v
7m 24s
20 v
9m 52s
80 v
12m 20s
250 v
14m 48s
800 v
17m 16 s
2300 v
19m 44s
Marker
D.C.
(b)

Figure 3

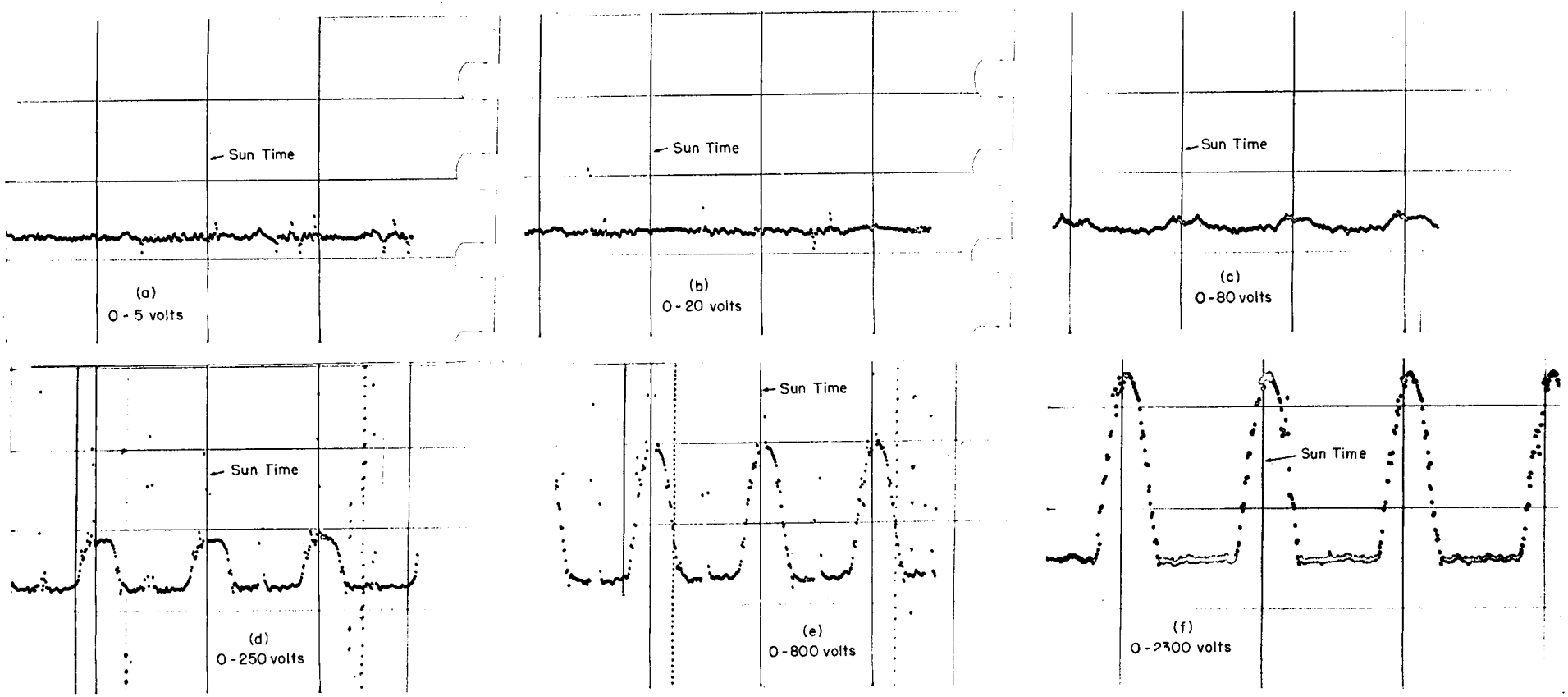
Sun Time
(a)
0 - 5 volts
Sun Time
(b)
0 - 20 volts
Sun Time
(c)
0 - 80 volts
Sun Time
(d)
0 - 250 volts
Sun Time
(e)
0 - 800 volts
Sun Time
(f)
0 - 2300 volts

Figure 4

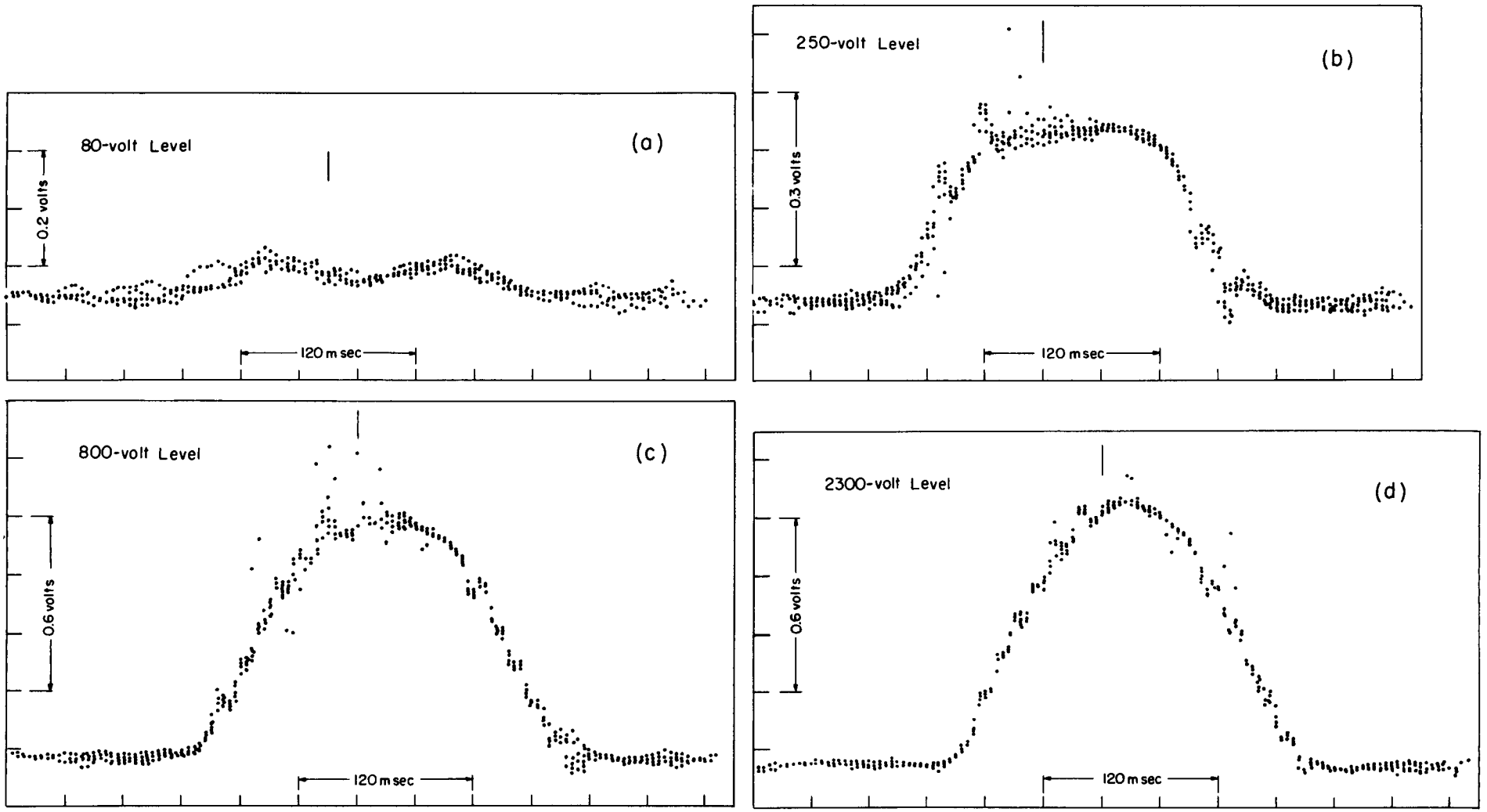
80-volt Level
(a)
0.2 volts
120 m sec
250-volt Level
(b)
0.3 volts
120 m sec
800-volt Level
(c)
0.6 volts
120 m sec
2300-volt Level
(d)
0.6 volts
120 m sec

Figure 5

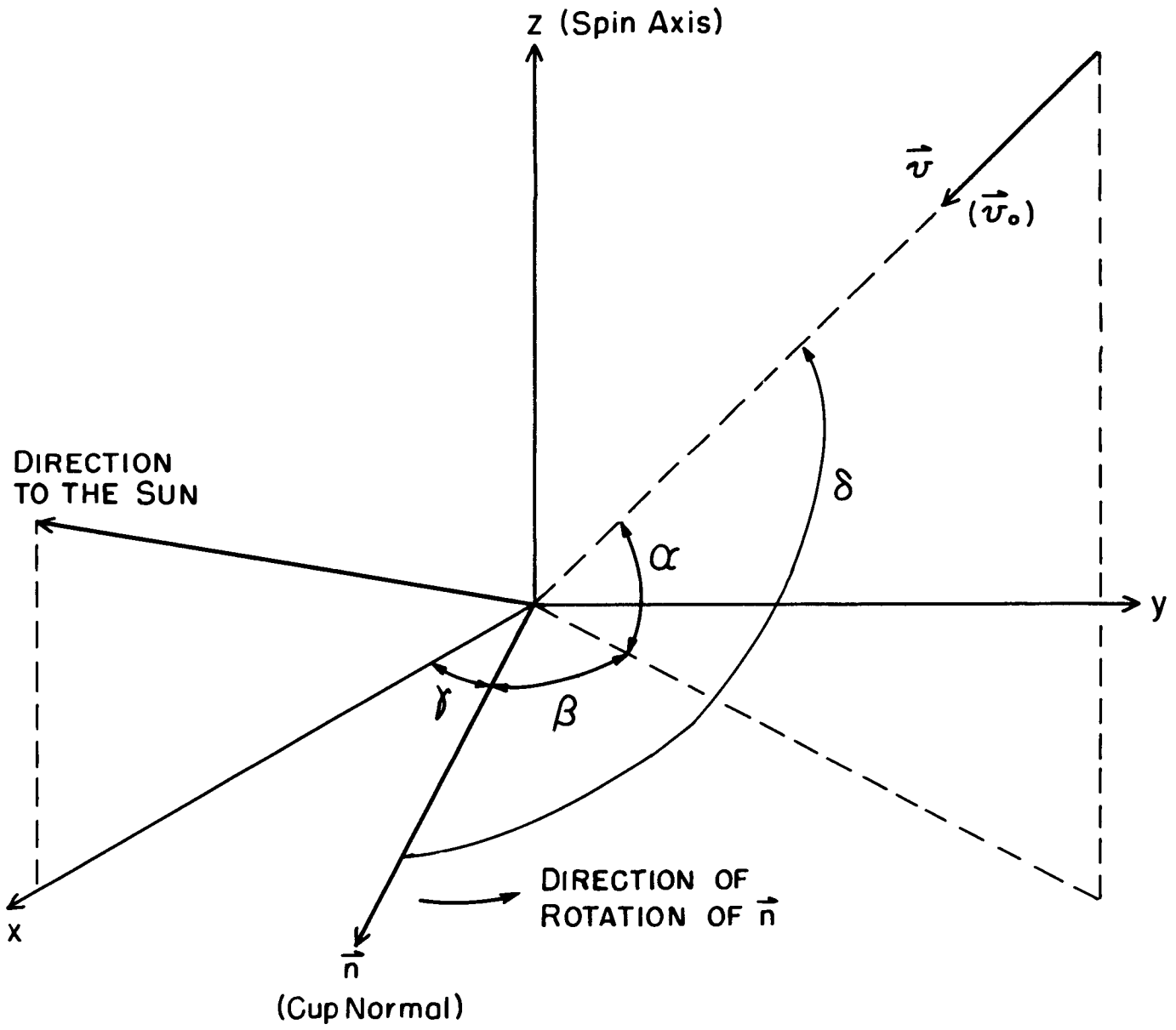
z (Spin Axis)
$\vec{v}$
$(\vec{v}_o)$
DIRECTION
TO THE SUN
δ
α
y
γ
β
x
DIRECTION OF
ROTATION OF $\vec{n}$
$\vec{n}$
(Cup Normal)

Figure 6

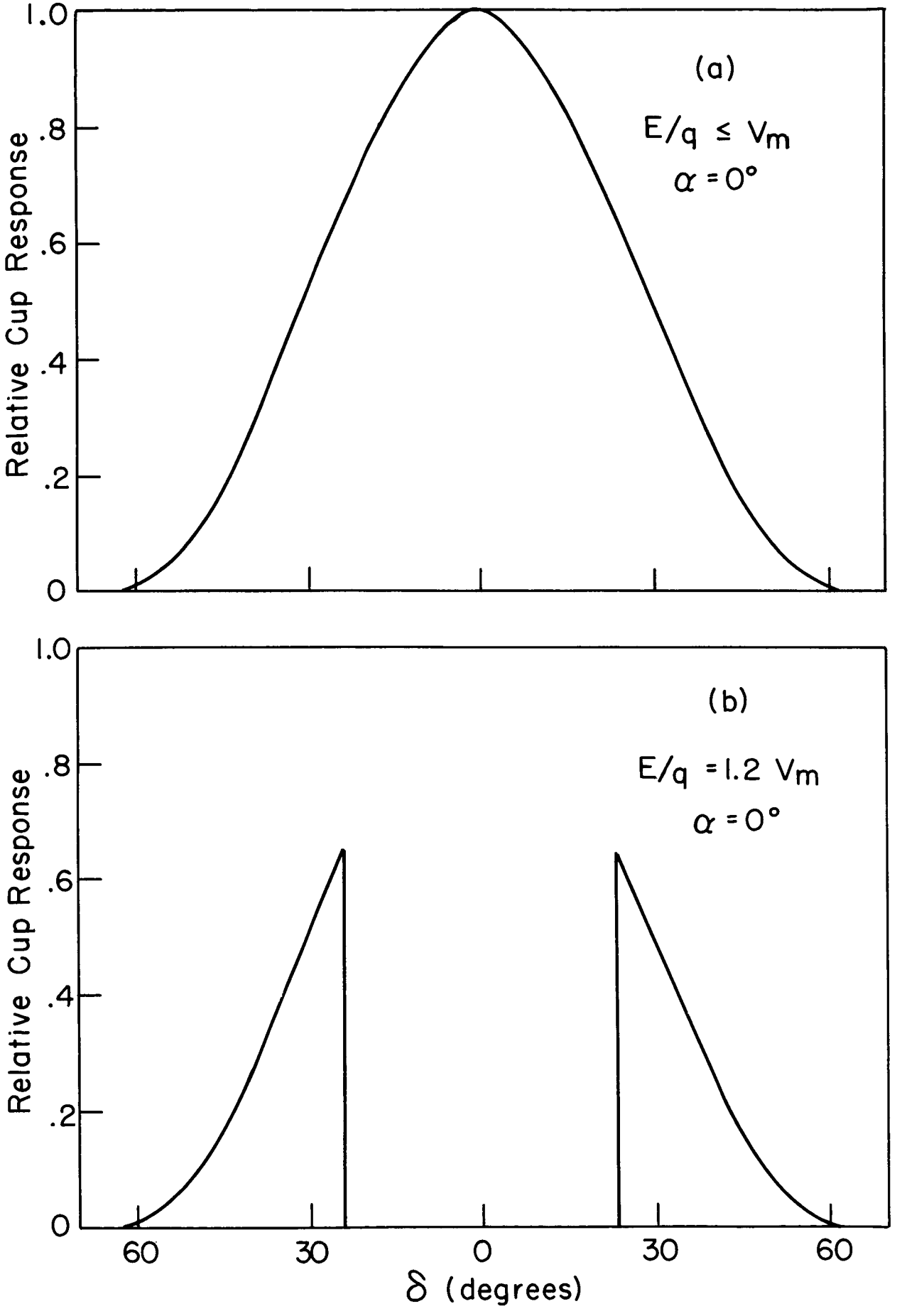
1.0
.8
.6
.4
.2
0
Relative Cup Response
(a)
E/q ≤ Vm
α = 0°
1.0
.8
.6
.4
.2
0
Relative Cup Response
(b)
E/q = 1.2 Vm
α = 0°
60
30
0
30
60
δ (degrees)

Figure 7

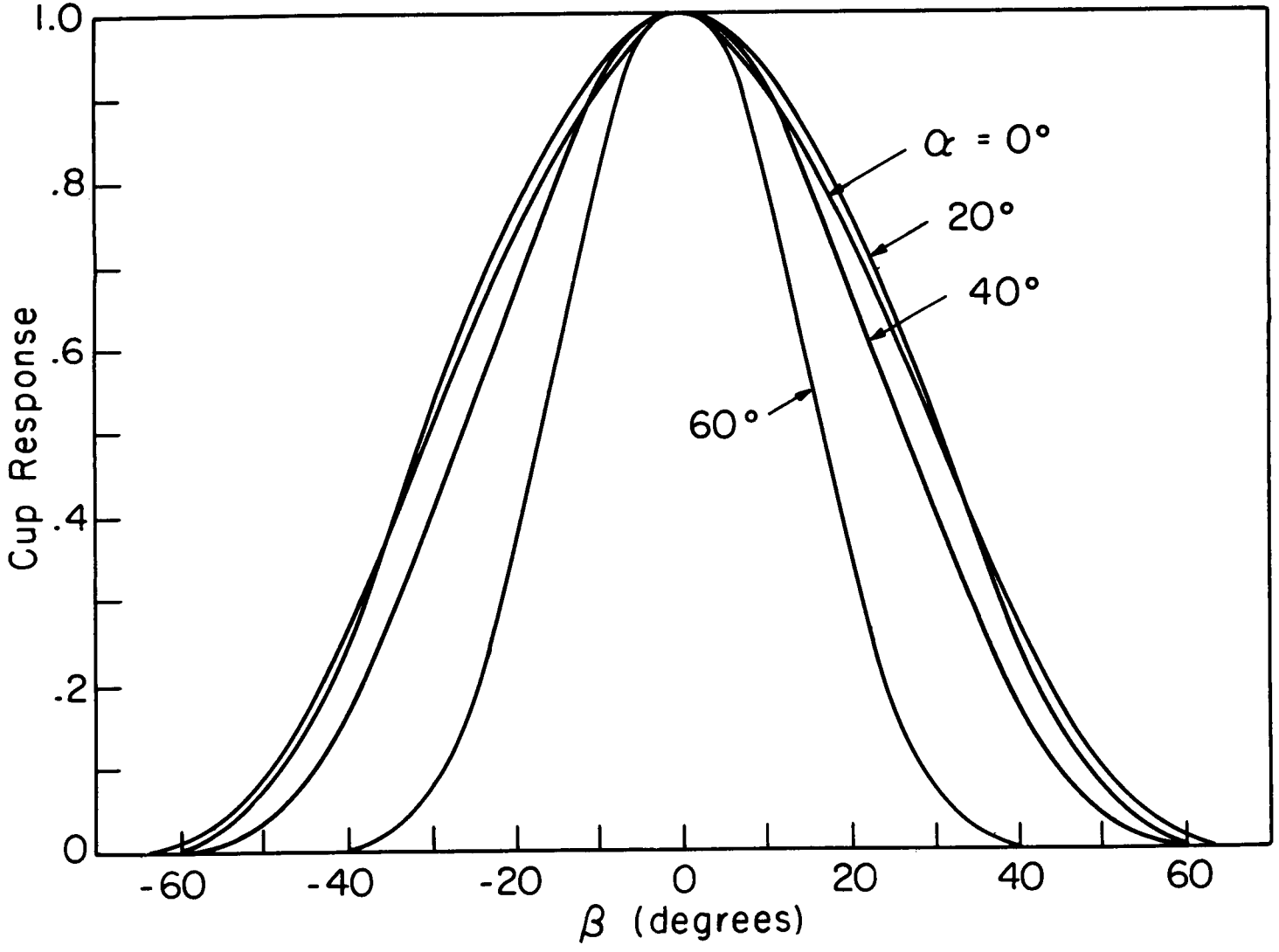

Figure 8

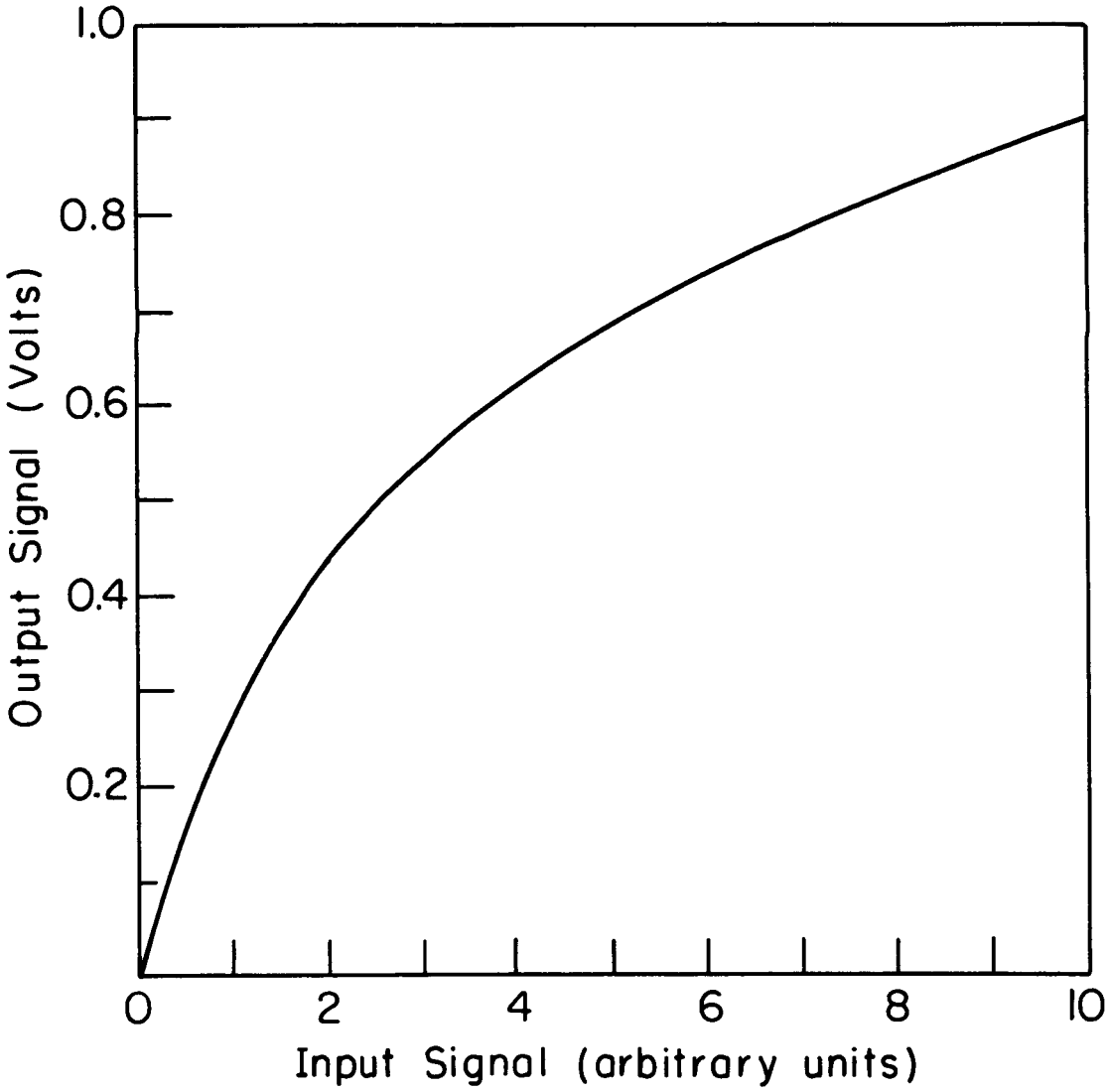
1.0
0.8
0.6
0.4
0.2
Output Signal (Volts)
0
2
4
6
8
10
Input Signal (arbitrary units)

Figure 9

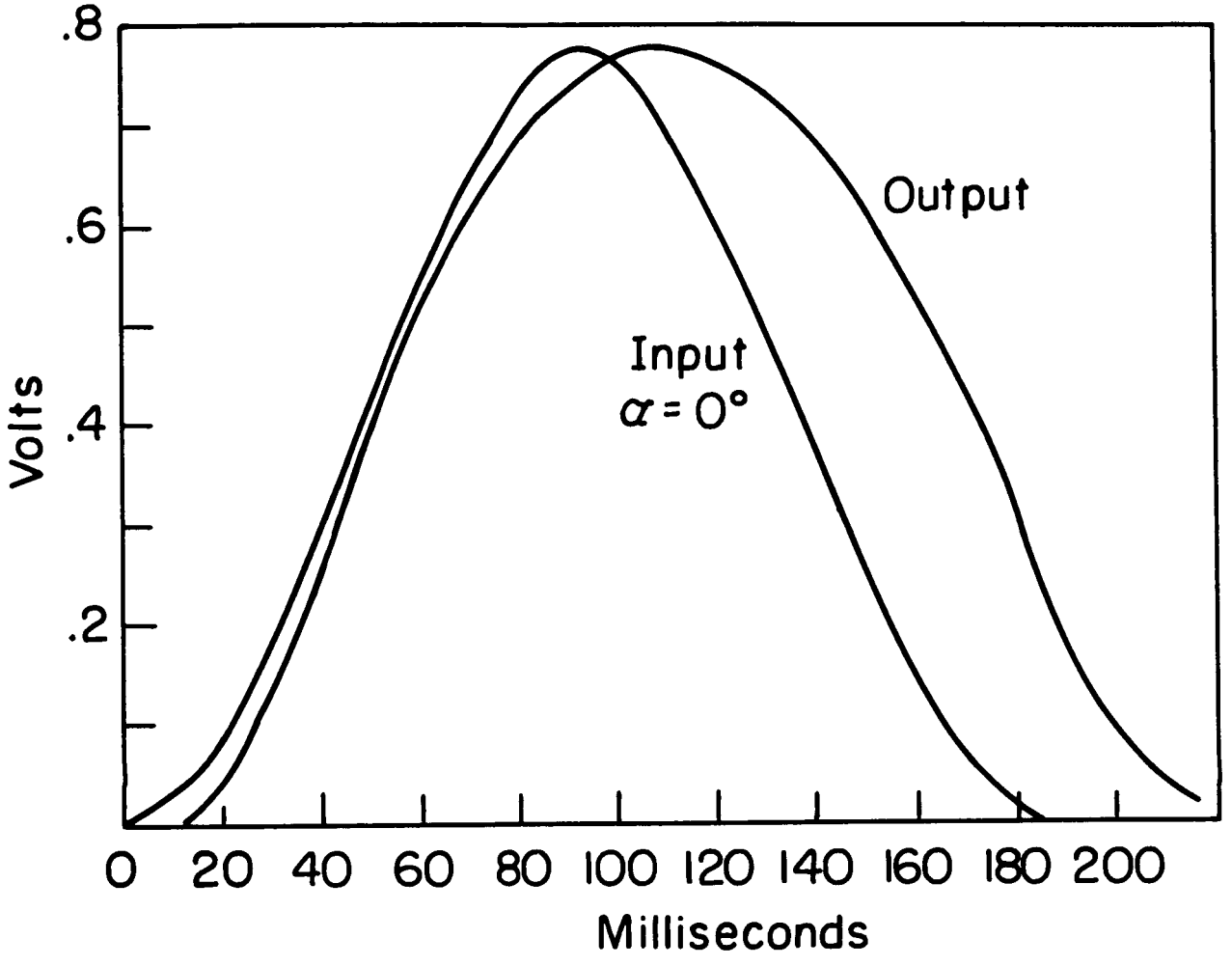
.8
.6
.4
.2
Volts
Output
Input
α = 0°
0 20 40 60 80 100 120 140 160 180 200
Milliseconds

Figure 10

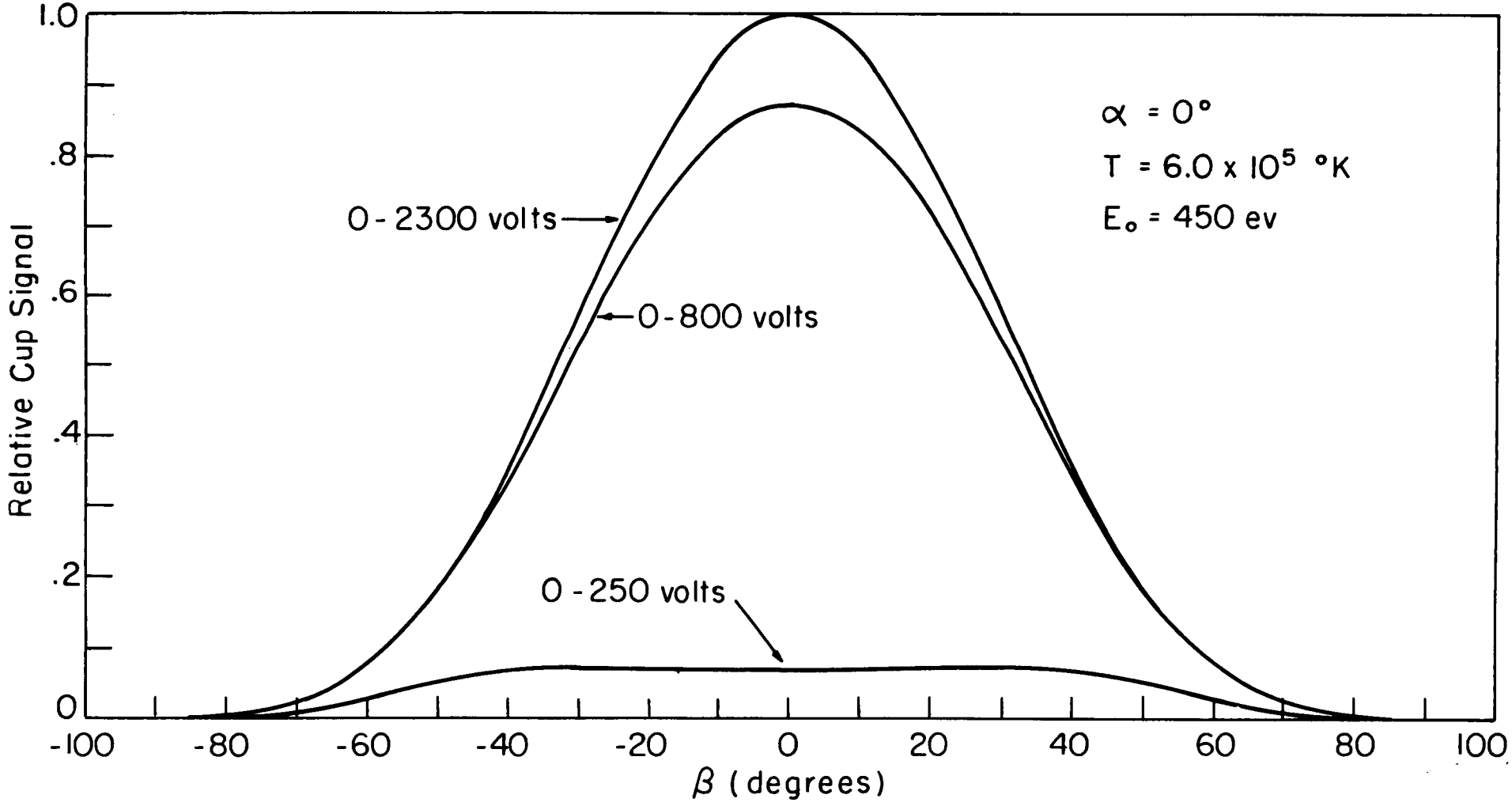
1.0
.8
.6
.4
.2
0
Relative Cup Signal
0 - 2300 volts
0 - 800 volts
0 - 250 volts
α = 0°
T = 6.0 x 10⁵ °K
E₀ = 450 ev
-100
-80
-60
-40
-20
0
20
40
60
80
100
β (degrees)

Figure 11

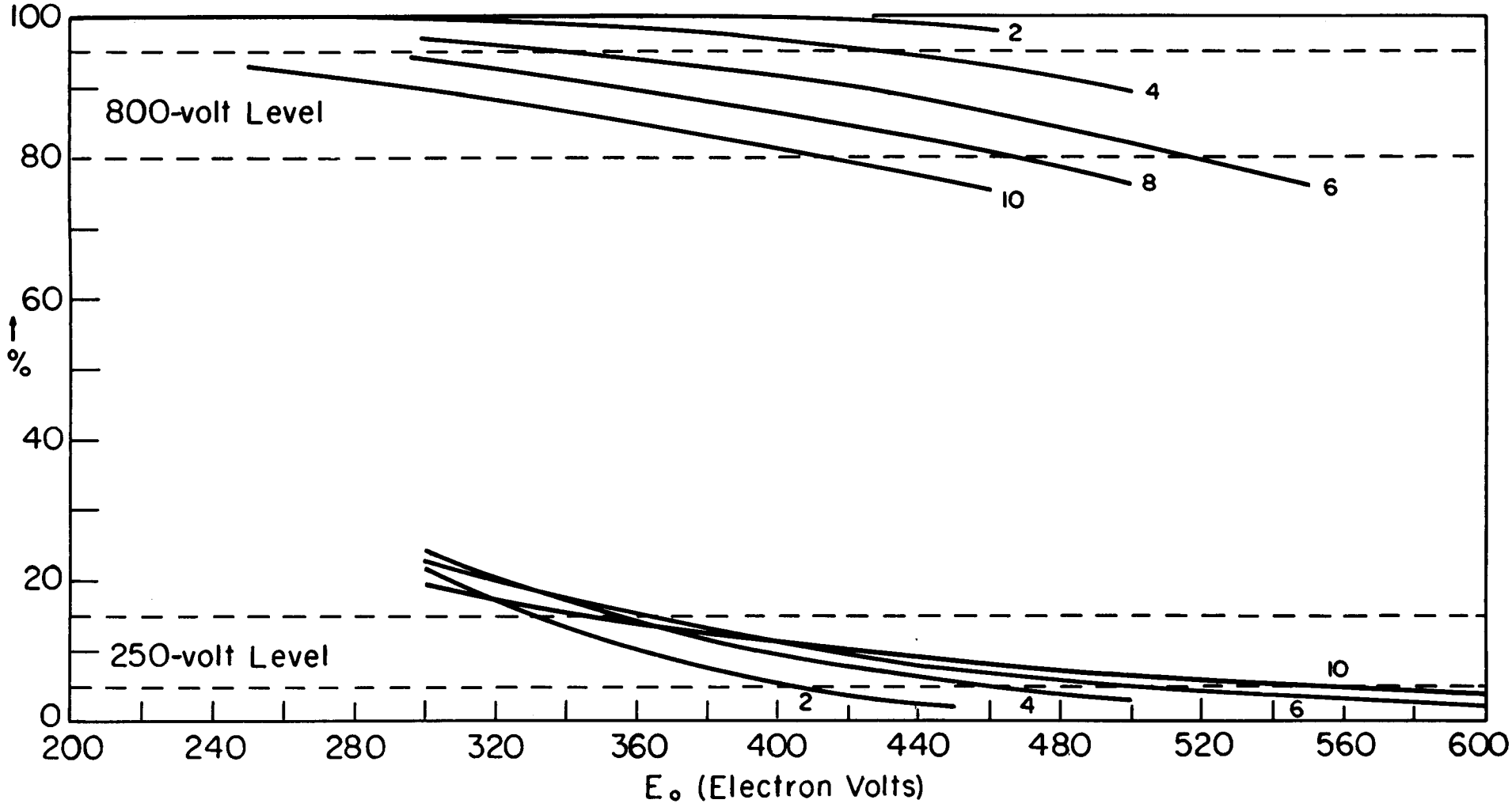
100
80
60
40
20
0
%
800-volt Level
250-volt Level
2
4
6
8
10
200
240
280
320
360
400
440
480
520
560
600
E₀ (Electron Volts)

Figure 12

0 - 800 VOLTS

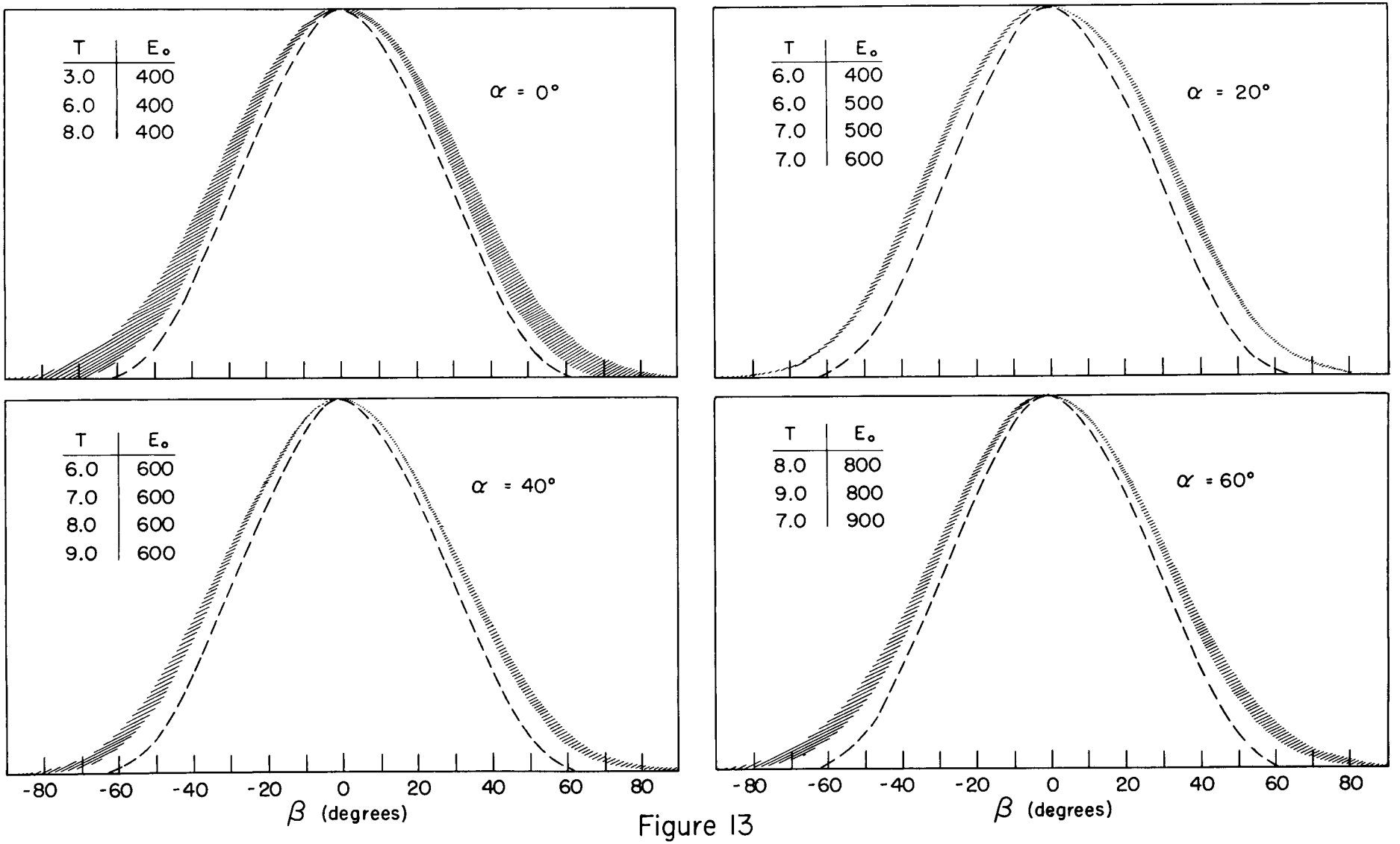

Figure 13

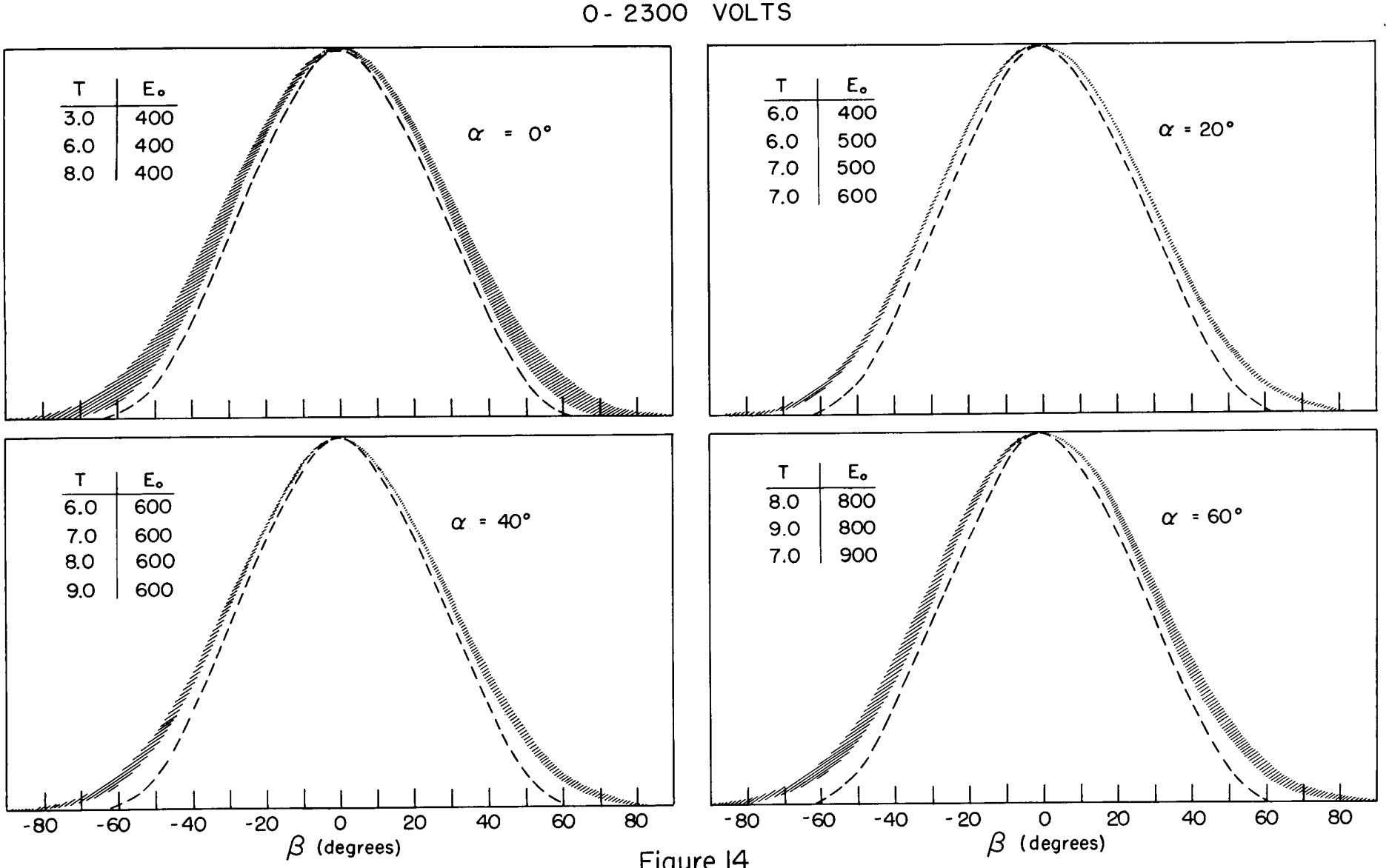
0 - 2300 VOLTS
T | Eo
3.0 | 400
6.0 | 400
8.0 | 400
α = 0°
T | Eo
6.0 | 400
6.0 | 500
7.0 | 500
7.0 | 600
α = 20°
T | Eo
6.0 | 600
7.0 | 600
8.0 | 600
9.0 | 600
α = 40°
T | Eo
8.0 | 800
9.0 | 800
7.0 | 900
α = 60°
-80 -60 -40 -20 0 20 40 60 80
β (degrees)
-80 -60 -40 -20 0 20 40 60 80
β (degrees)

Figure 14

0 - 250 VOLTS

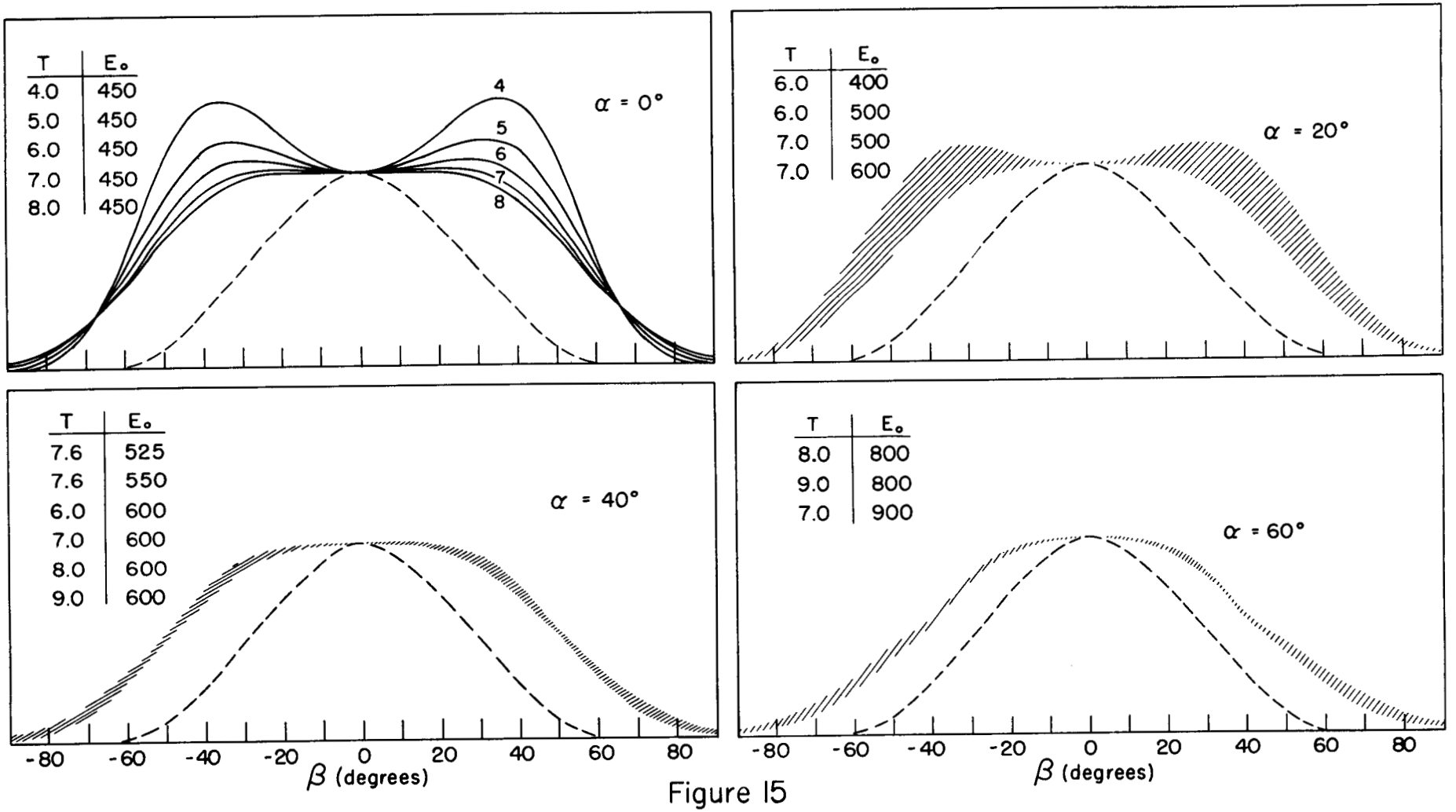

Figure 15

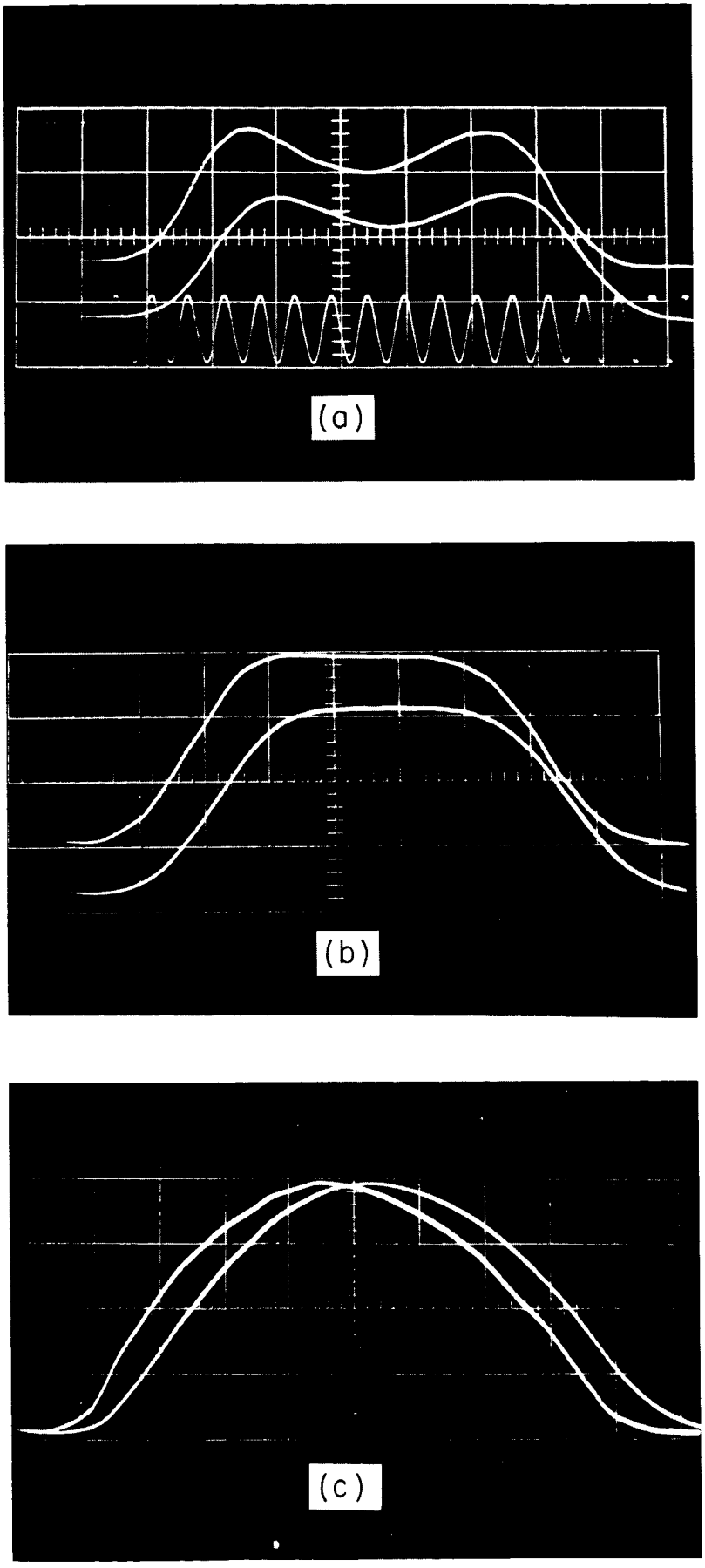

Figure 16

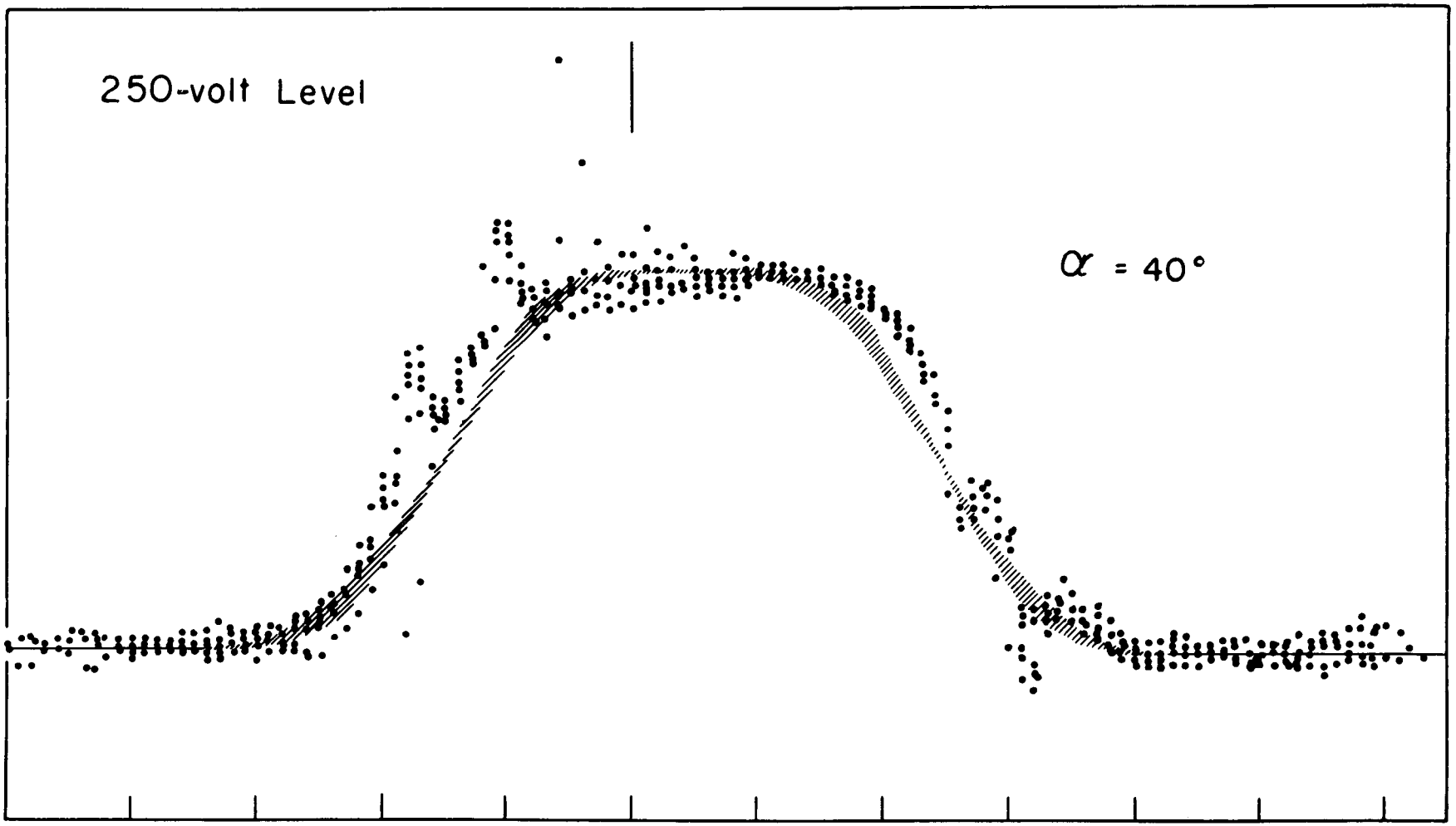

Figure 17

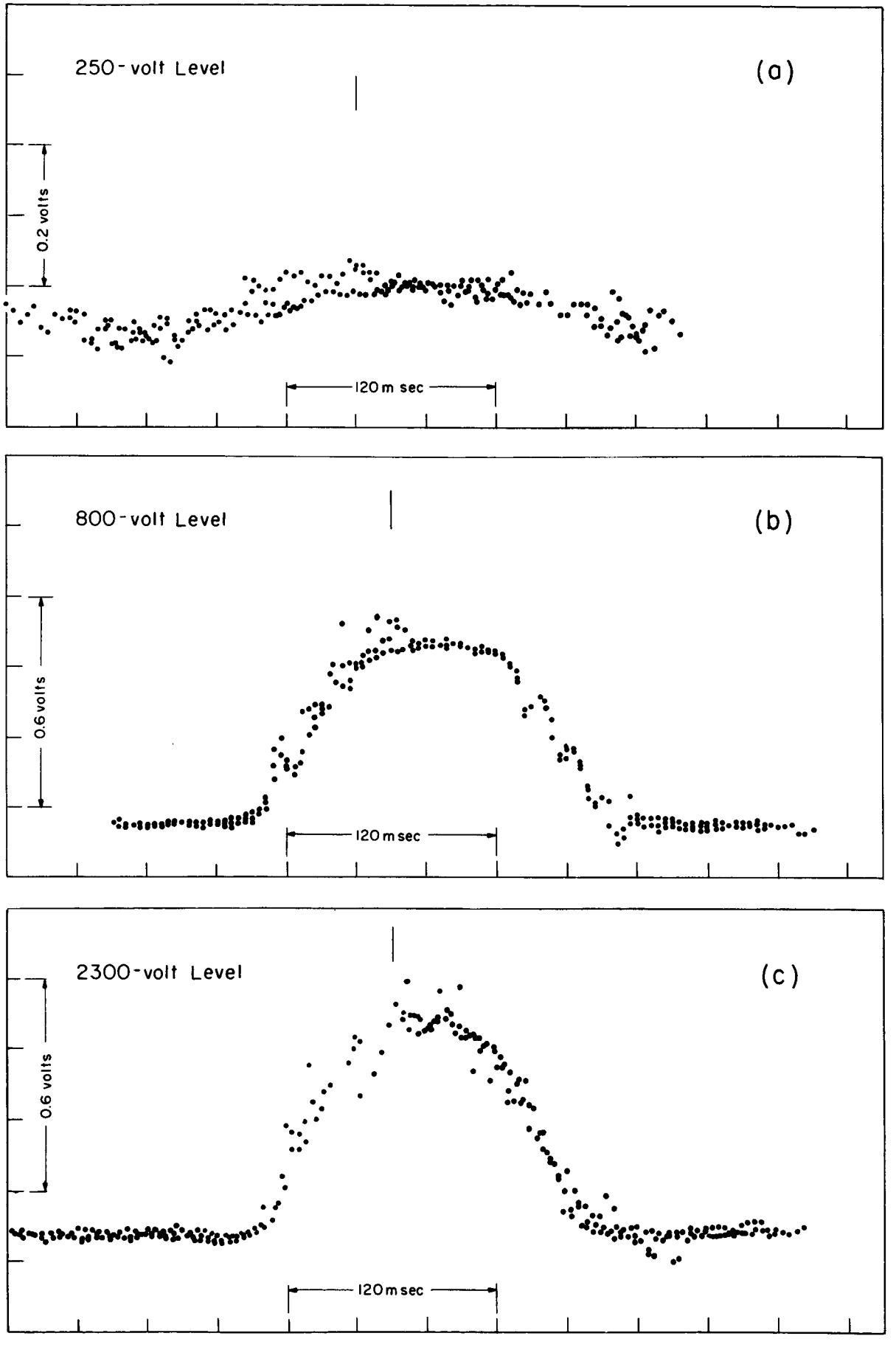
250-volt Level
(a)
0.2 volts
120 m sec
800-volt Level
(b)
0.6 volts
120 m sec
2300-volt Level
(c)
0.6 volts
120 m sec

Figure 20

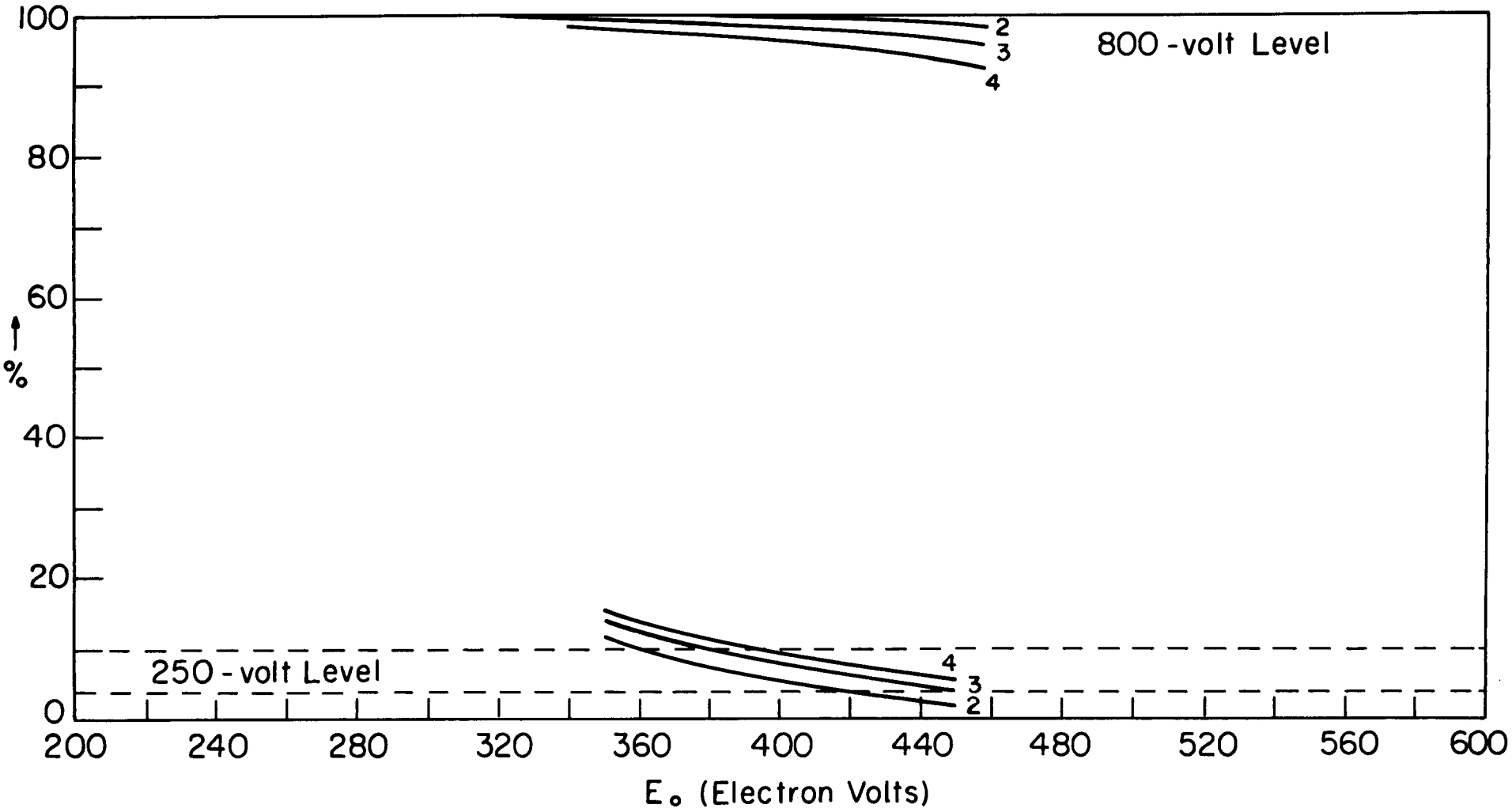
100
80
60
%
40
20
0
800 - volt Level
2
3
4
250 - volt Level
4
3
2
200
240
280
320
360
400
440
480
520
560
600
E₀ (Electron Volts)

Figure 21

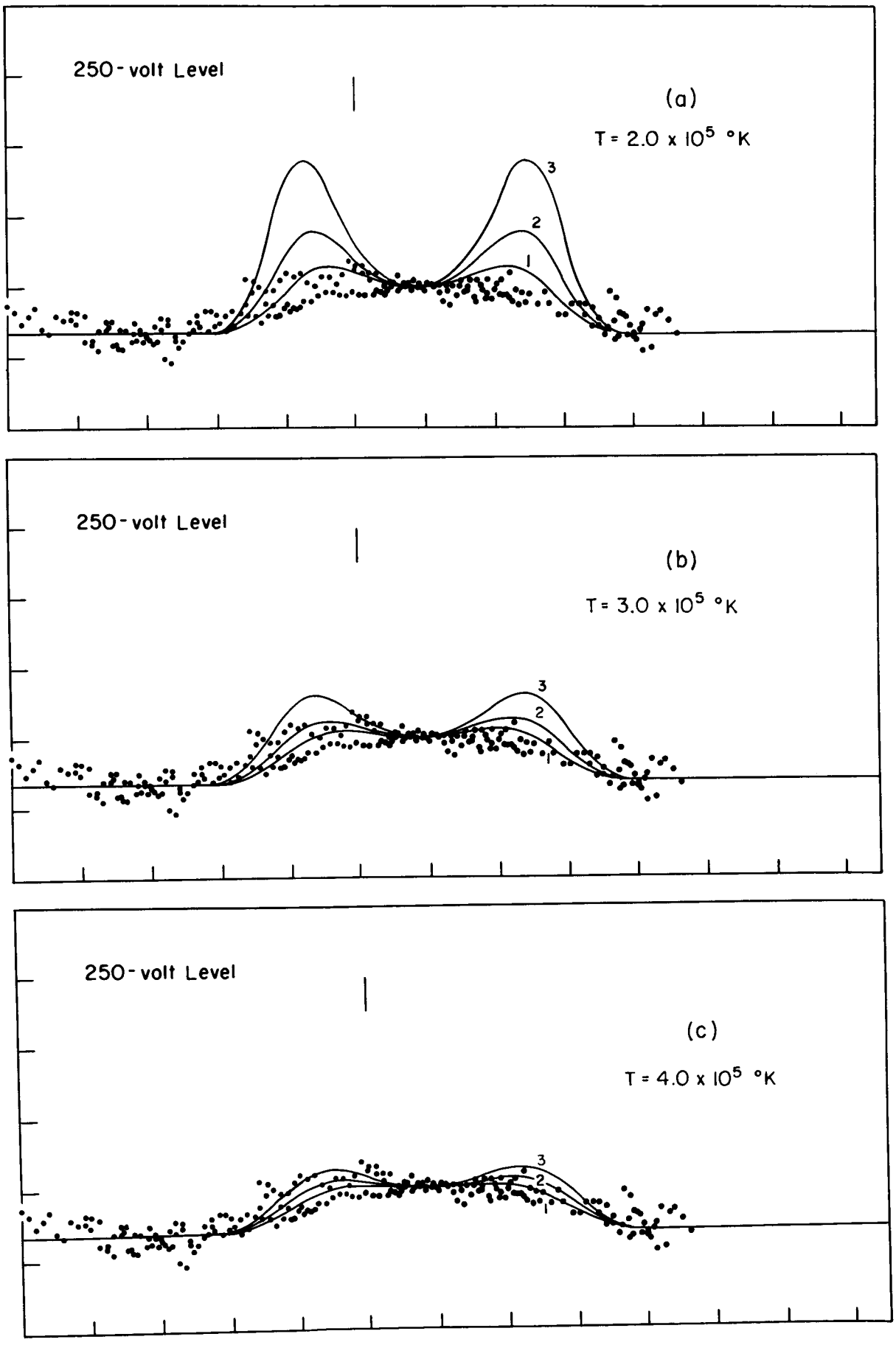
250-volt Level
(a)
T = 2.0 x 10^5 °K
3
2
1
250-volt Level
(b)
T = 3.0 x 10^5 °K
3
2
1
250-volt Level
(c)
T = 4.0 x 10^5 °K
3
2
1

Figure 22

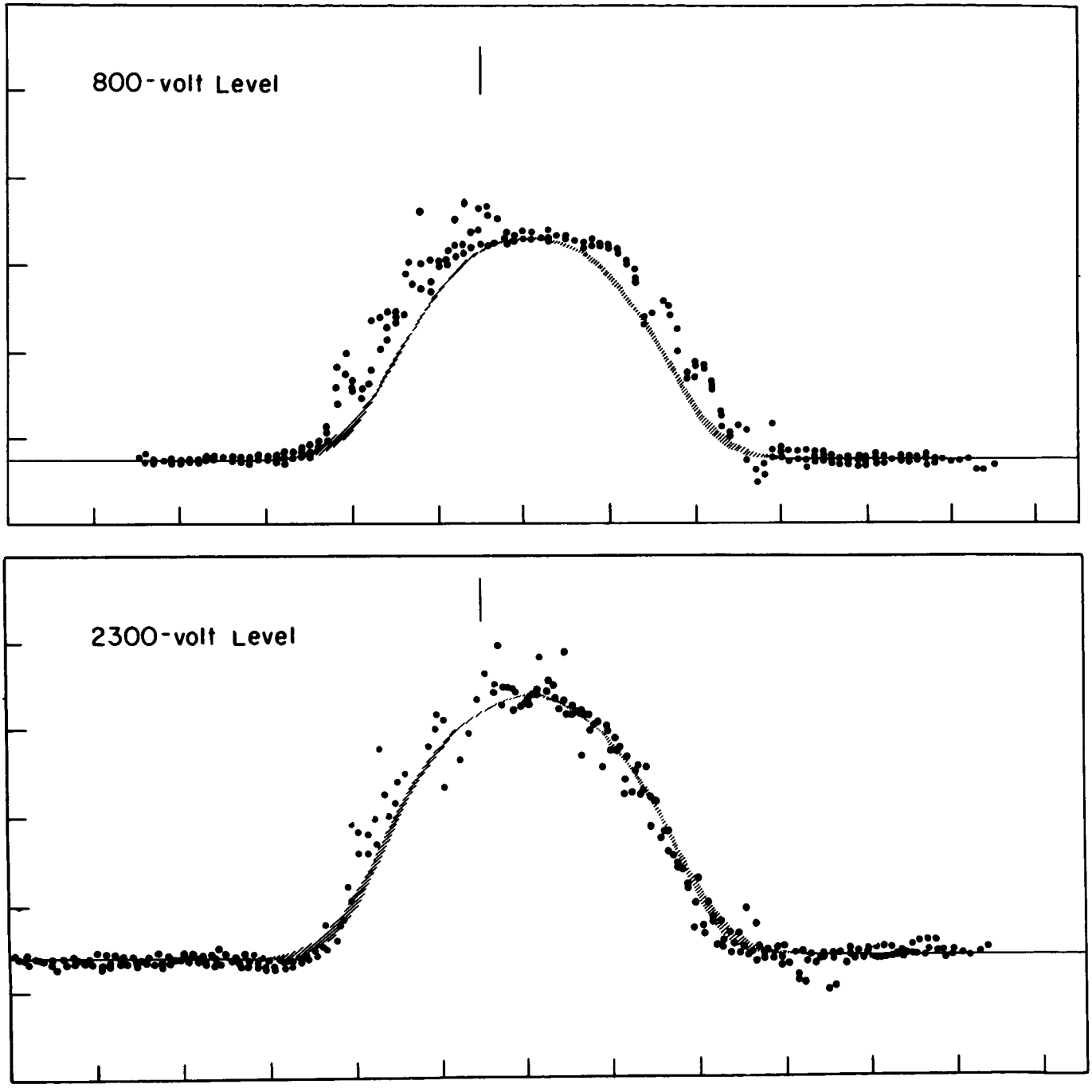

Figure 23

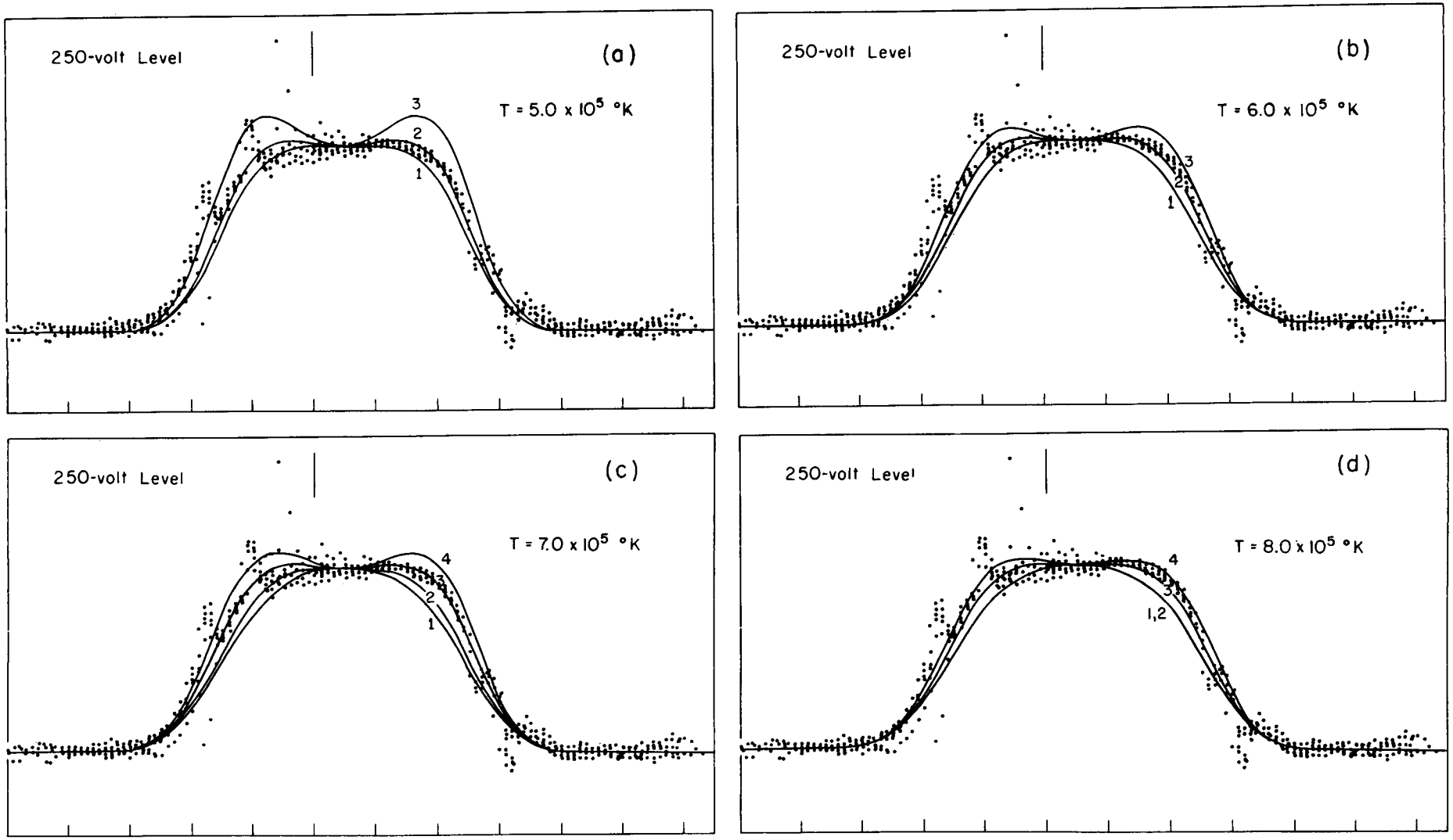
250-volt Level
(a)
T = 5.0 x 10^5 °K
3
2
1
250-volt Level
(b)
T = 6.0 x 10^5 °K
3
2
1
250-volt Level
(c)
T = 7.0 x 10^5 °K
4
3
2
1
250-volt Level
(d)
T = 8.0 x 10^5 °K
4
3
1,2

Figure 18

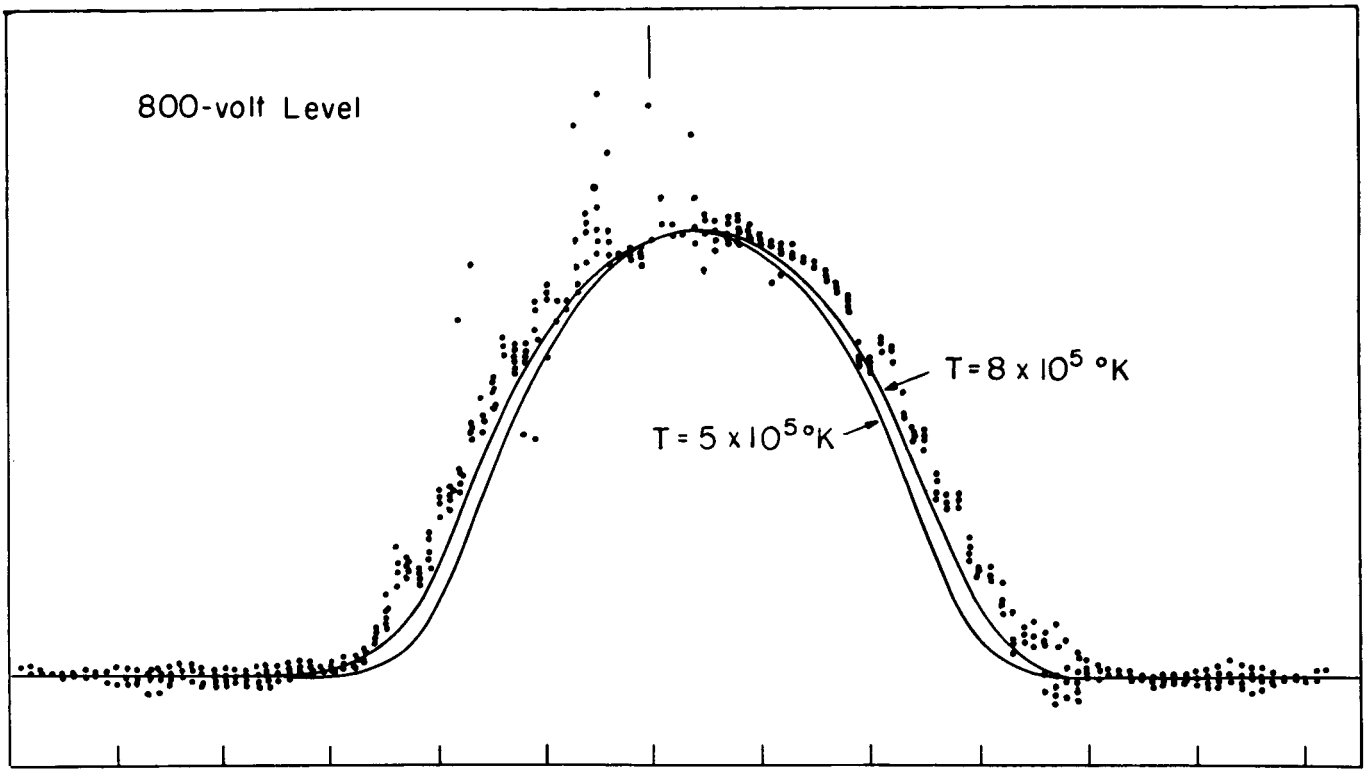
800-volt Level
T = 8 x 10^5 °K
T = 5 x 10^5 °K

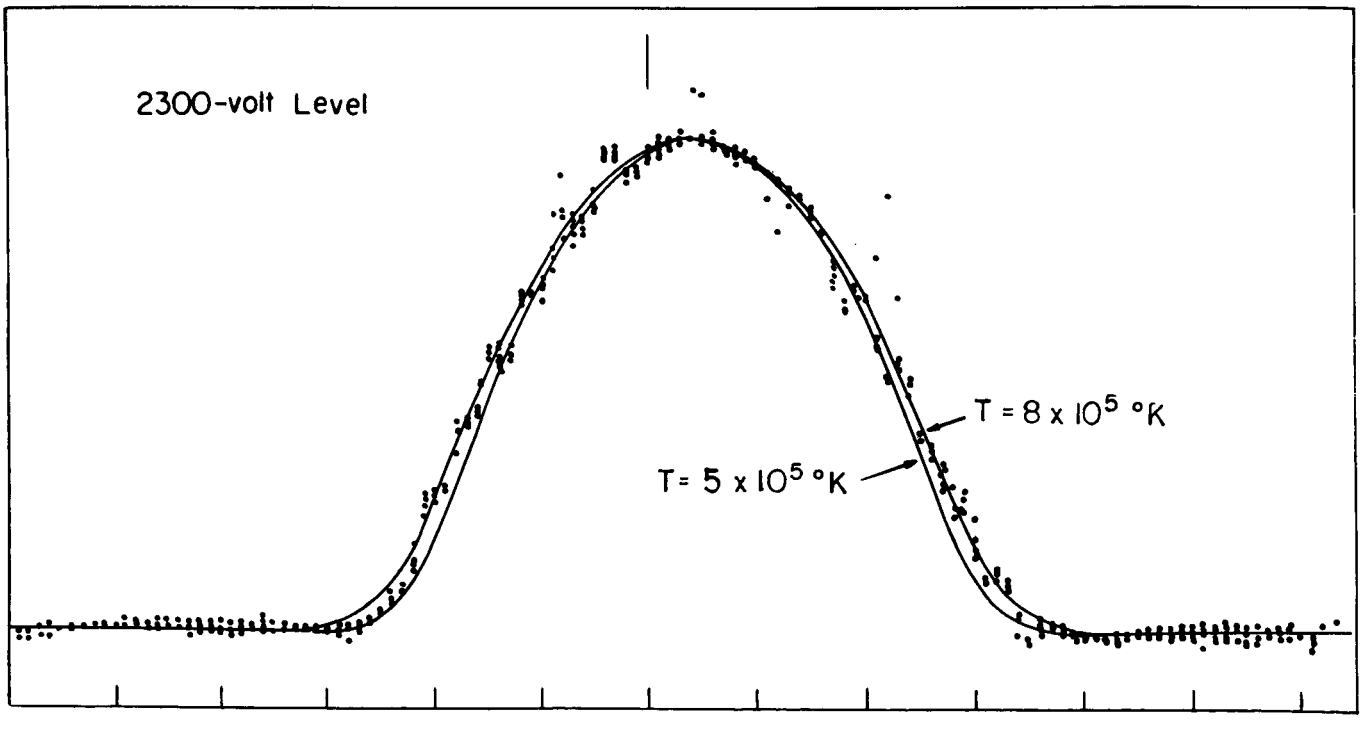
2300-volt Level
T = 8 x 10^5 °K
T = 5 x 10^5 °K

Figure 19

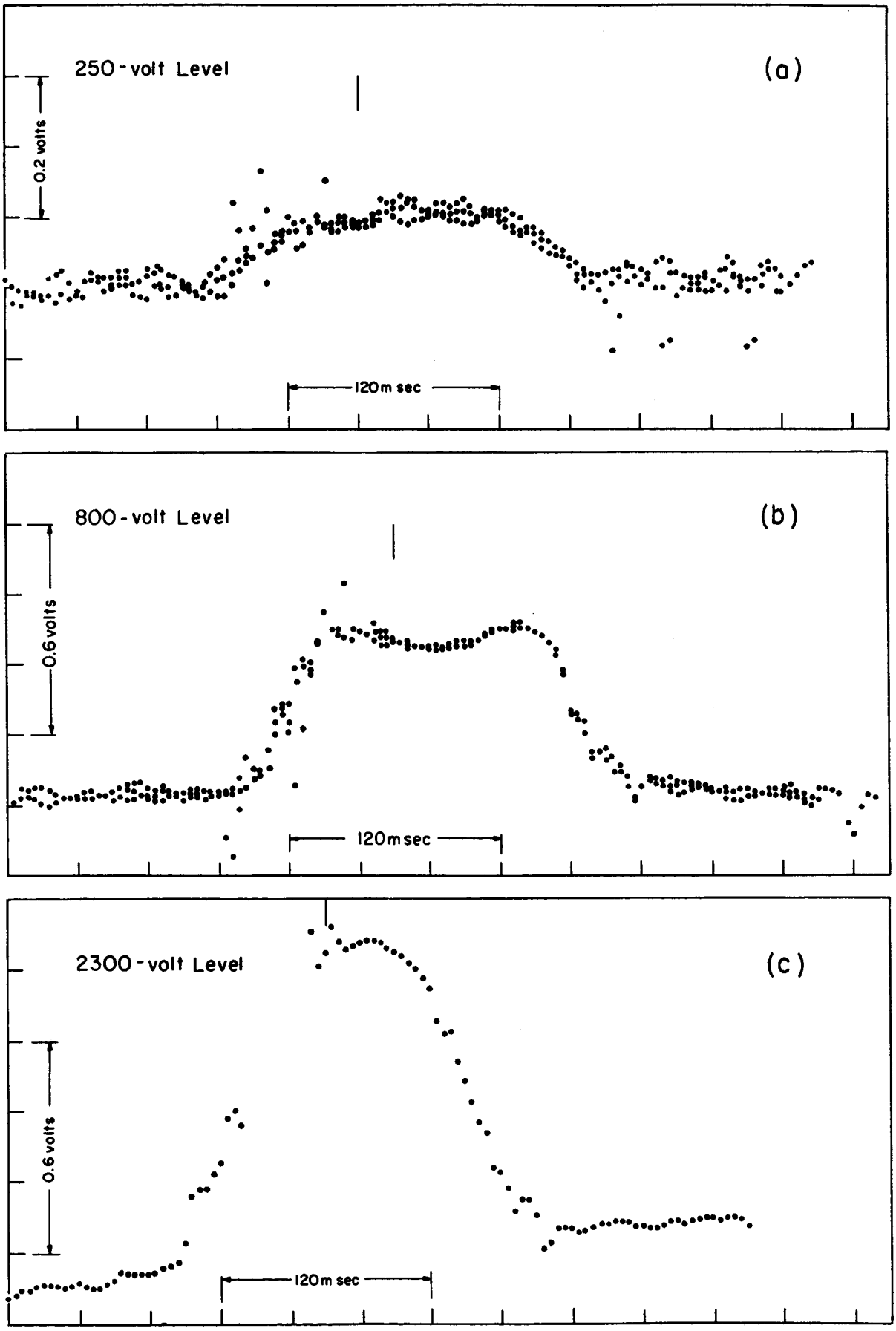
250-volt Level
(a)
0.2 volts
120m sec
800-volt Level
(b)
0.6 volts
120m sec
2300-volt Level
(c)
0.6 volts
120m sec

Figure 24

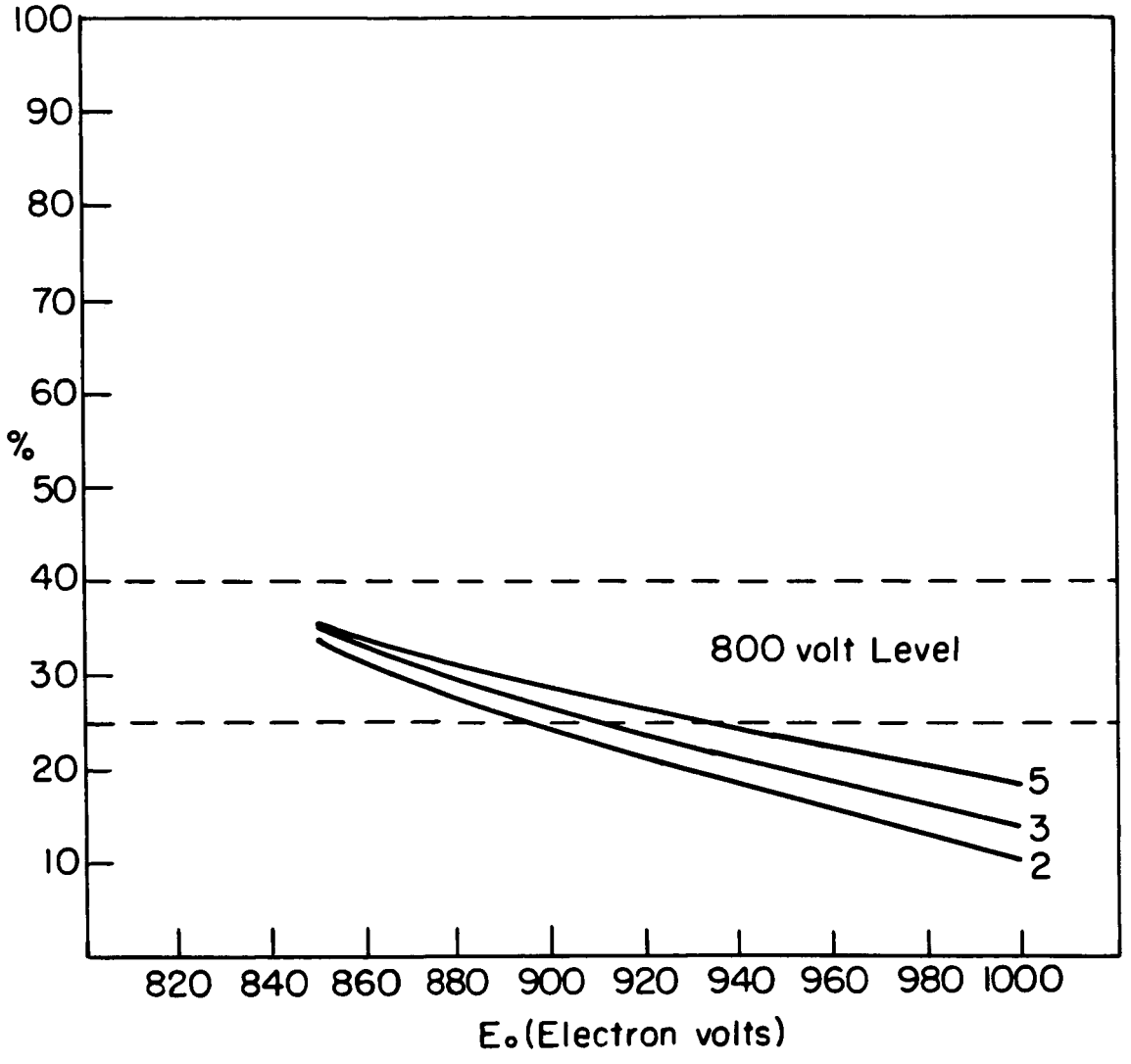
100
90
80
70
60
%
50
40
30
20
10
800 volt Level
5
3
2
820 840 860 880 900 920 940 960 980 1000
Eo (Electron volts)

Figure 25

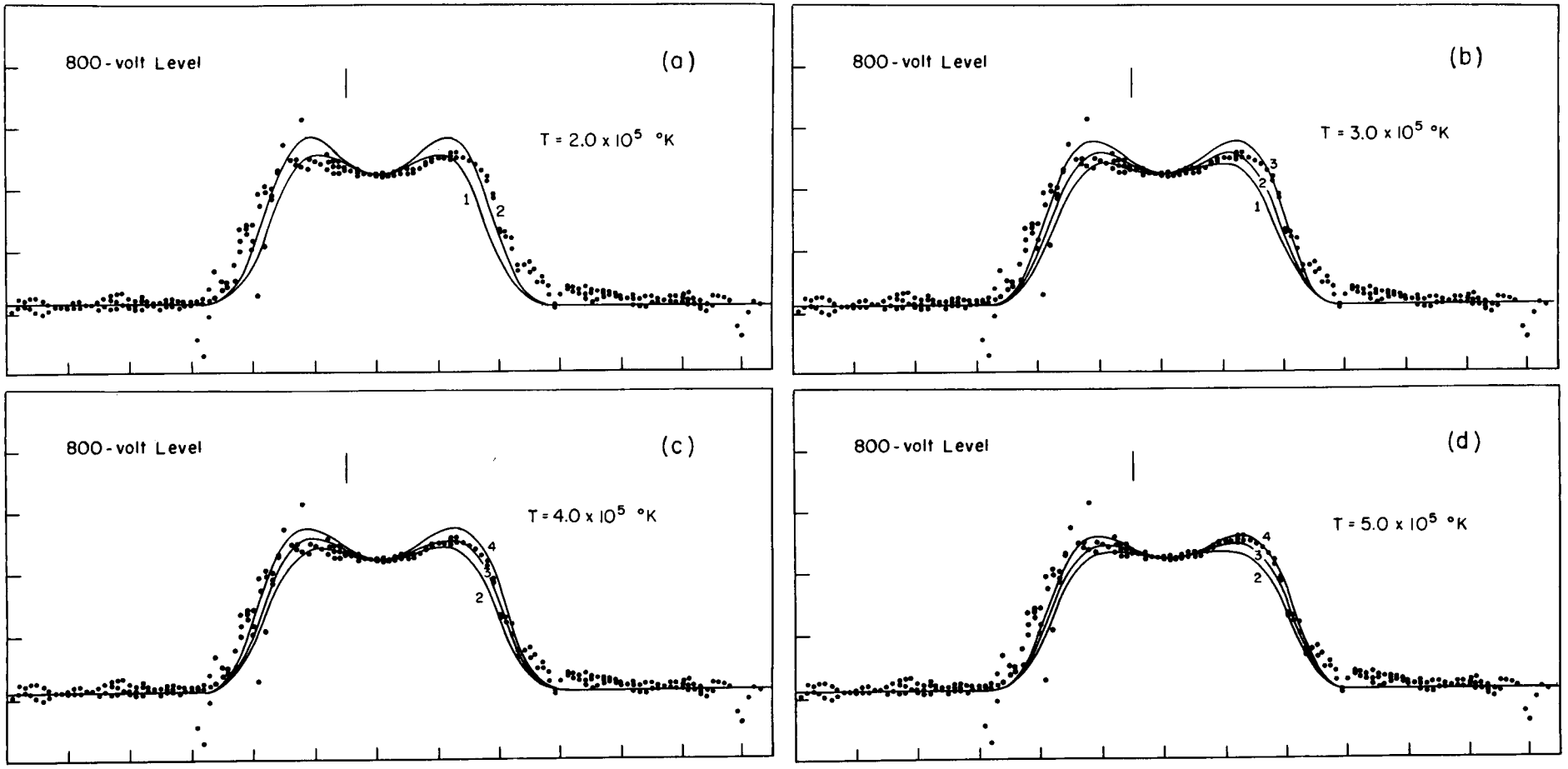
800-volt Level
(a)
T = 2.0 x 10^5 °K
1
2
800-volt Level
(b)
T = 3.0 x 10^5 °K
1
2
3
800-volt Level
(c)
T = 4.0 x 10^5 °K
2
3
4
800-volt Level
(d)
T = 5.0 x 10^5 °K
2
3
4

Figure 26

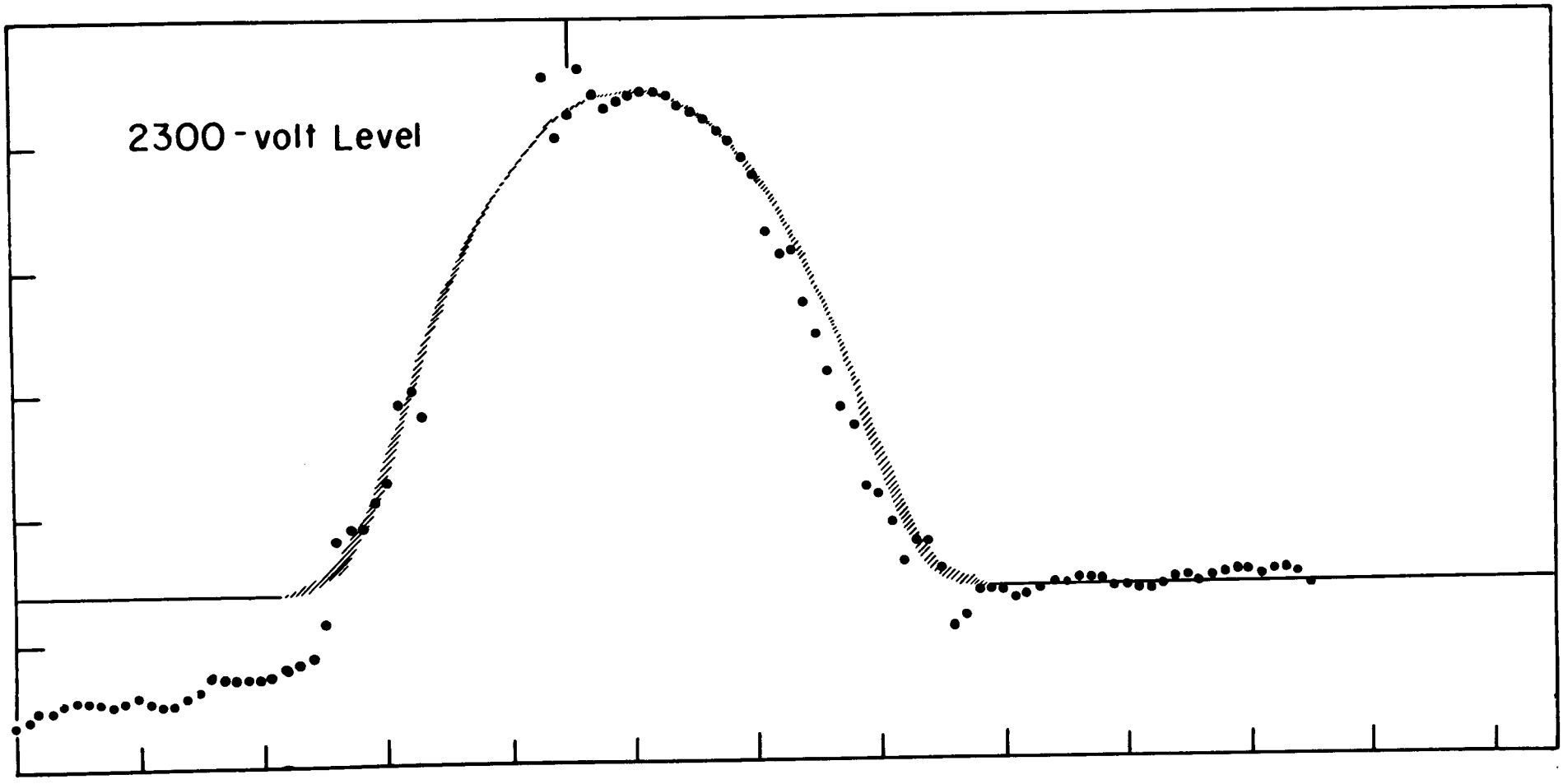

Figure 27